HOKKAIDO UNIVERSITY

Title	Surface-nitrogen Removal Studied from Desorption Dynamics
Author(s)	Kobal, Ivan; Kokalj, Anton; Horino, Hideyuki; Ohno, Yuichi; Matsushima, Tatsuo
Citation	Trends in Chemical Physics, 10, 139-178
Issue Date	2002
Doc URL	http://hdl.handle.net/2115/14617
Rights	Copyright (c) 2002 Research Trends
Type	article (author version)
File Information	Trend 2002 Surface nitrogen removal.pdf

Instructions for use

Surface-nitrogen Removal Studied from Desorption Dynamics

Ivan Kobal and Anton Kokalj
J. Stefan Institute, 1000 Ljubljana, Slovenia

Hideyuki Horino, Yuichi Ohno and Tatsuo Matsushima*
Catalysis Research Center, Hokkaido University, Sapporo 060, Japan

ABSTRACT

The removal of adsorbed nitrogen from catalyst surfaces is one of the key processes in proceeding efficient catalytic treatments of nitrogen oxides in exhaust gases from automotive and stationary sources. This review summarizes the typical characteristics of three removal processes of surface-nitrogen on metal surfaces, i.e., (i) $2N(a) \rightarrow N_2(g)$, (ii) $N(a) + NO(a) \rightarrow N_2O(a) \rightarrow N_2(g) + O(a)$ and (iii) $NO(a) + O(a) \rightarrow NO_2(a) \rightarrow NO^-_3(a) \rightarrow N_2(g)$. In the first process desorbing N_2 is collimating along the surface normal direction and is vibrationally excited because a large amount of the binding energy is released in the associative process. N_2 in the second process collimates into a highly inclined direction on flat surfaces because N_2O lies on the surface immediately before dissociation. These characteristics are exemplified to be useful to examine the reaction pathway of NO_X decomposition on catalysts.

1. INTRODUCTION

Nitrogen oxides are produced in automotive and stationary devices burning fossil fuel [1,2,3]. Because of increasingly stringent restrictions on emission [4], their abatement is a serious technological concern. In cars, whose exhaust contributes about one-third to the total NO emission in developed countries, the so-called three-way catalyst (TWC) is designed to simultaneously convert CO, NO and unburned hydrocarbons into environmentally harmless substances [5]. The conversion, depending on the operational regime, is not always complete and undesirable by-products (mostly N_2O and NO_2) are concomitantly evolved [3]. Although the kinetics and reaction mechanism of these conversion reactions on noble metals, which are the active catalytic constituents of the converters, are known in general, there are disagreements concerning some points, and still some details remain to be explained [6].

NO dissociation, the key reaction step, is retarded by oxygen and nitrogen adspecies, products left from dissociation on the catalyst surface. Their elimination is therefore crucial to continue the conversion cycle. While O(a) is consumed by CO, hydrogen, or hydrocarbons, the process of elimination of adsorbed nitrogen is not clear yet. It may proceed *via* the associative desorption $2N(a) \rightarrow N_2(g)$ in a wide temperature range or *via* the associative reaction and decomposition as a $N(a) + NO(a) \rightarrow N_2O(a) \rightarrow O(a) + N_2(g)$ reaction at low temperatures [7,8]. Despite extensive studies applying isotope thermal desorption spectroscopy, these two processes have not been differentiated yet [9,10]. Since N_2 desorbing in NO and N_2O decompositions [11,12,13] and in the recombinative

desorption of N(a) [14] on noble metal surfaces was found to carry a high excess of translational energy, this indicates that it stores information about the orientation and symmetry of the reaction site and hence of the position and geometry of the transition state. Thus, the application of SSDD (site-sensitive desorption dynamics) seems desirable to tackle the above differentiation [15,16,17,18].

We report here the spatial and velocity distributions of desorbing products in decomposition of nitrogen oxides in both thermal desorption and steady-state reaction mainly on Pd, Ir, and Rh single-crystal surfaces. To start with, the principles of desorption dynamics are briefly presented on the basis of hydrogen associative desorption from copper surfaces. Modern desorption dynamics have been mostly established in studies of this system, yielding the principal concepts of repulsive desorption. During an adsorption or desorption process, the kinetic energy of the molecule involved may be changed, and, also, its internal degrees of freedom might be affected. The processes may also be accompanied by electron-hole pair excitation and the coupling of molecular motions with the surface phonons. Here, the H_2 molecule shows some advantages relative to molecules such as CO, CO_2, NO, N_2. Because of its low electron affinity, electron-hole pair excitation plays a less important role than it would in other systems [19], and, because of its low molecular mass compared to the mass of the Cu atom, the coupling of H_2 vibrational modes with the surface phonons may be neglected [20,21]. Therefore, the H_2/Cu system as a repulsive desorption model has been thoroughly studied both experimentally and theoretically.

2. STATUS OF DESORPTION DYNAMICS

Dissociative adsorption of hydrogen on copper surfaces is a good example of activated adsorption [22,23]. In the reverse process, i.e. the recombination reaction as $2H(a) \rightarrow H_2(g)$, hydrogen is repulsively desorbed from the surface.

We may classify the development of the investigations of hydrogen recombinative desorption dynamics into three stages: (i) measurements of the angular and velocity distribution at fixed azimuth, (ii) state-resolved analysis of adsorption and desorption assisted by quantum mechanical calculations, and (iii) an attempt to find surface structure dependence. In the first generation, after the pioneering work by Stickney's group [24,25], the angular and velocity distributions were mostly measured at a fixed crystal azimuth. Attempts were made to explain the results within one-dimensional activation barrier models [26,27]. However, there were difficulties in explaining aspects such as the angle-dependence of the translational energy of desorbing molecules, a wide range of

the threshold energy required for H_2 dissociation, and the relatively broad angular distribution of desorbing H_2 in the reverse process compared with the high threshold energy for dissociation.

The second generation was opened by state-resolved adsorption and desorption measurements using molecular beams [28,29,30] and REMPI (resonance-enhanced multi-photon ionization) [31] techniques. The dissociation probability was shown to depend on the vibrational state of the incident molecules. The threshold kinetic energy for dissociation was clearly and significantly reduced when the molecules were vibrationally excited [32,33]. Furthermore, in the recombinative desorption, the vibrationally excited molecules have lower translational energy [34,35]. In both dissociation and recombination events, the energy of the reactant was shown to be converted into translational, vibrational, and rotational modes. The extent of this conversion depends on the shape of PES (potential energy surface). In particular, details of conversion depend on the molecular orientation on the surface. At this stage, it became clear that at least two-dimentional PES is needed to describe the energy conversion into different degrees of freedom.

In the second generation, theoretical work also contributed largely to the understanding of the desorption dynamics. Different levels of the quantum mechanical treatment have been applied [36,37,38,39,40,41,42,43,44,45,46]. The most sophisticated calculations treat the H_2 adsorption-desorption quantum mechanically as a 6D (six-dimensional) problem [47,48,49,50,51,52,53] applying DFT (density functional theory) with a slab presentation of the solid surface. The name originates from six coordinates to describe the system: three external coordinates for the position of the center of mass with respect to the solid surface and three internal coordinates of the H_2 molecule (inter-atomic distance, polar, and azimuth angle). PES is constructed for different adsorption-desorption sites (see, for example, Fig. 13 in Ref. [50]). Although the calculations do not always reproduce the numerical values of the experimentally determined variables, they show correct trends of relationships among them. More importantly, they provide the physical and chemical grounds to understand these trends and often give information not available from the experiments.

2.1 Detailed energy conversion

Calculations show that the barrier for H_2 dissociation on copper is located late along the reaction coordinate, in the *exit channel*, where the H-H bond is already significantly elongated [39,54]. This enables translation-vibration coupling, resulting in the conversion of translational energy into vibrational energy [55,42,56], the process being governed by the curvature of the PES [54]. This supports the

experimental observation that the dissociative adsorption probability is higher for vibrationally excited H_2 molecules [34,33]. In the reverse process, desorbing H_2 molecules in vibrationally excited states have less translational energy [42]. This energy conversion is sensitive to the molecule orientation towards the surface. The translation-vibration coupling is much more pronounced for the *helicopter* H_2 molecules (with the molecular axis oriented parallel to the surface) than for *cartwheel* H_2 molecules (with the molecular axis oriented perpendicular to the surface) [51,57]. This phenomenon causes *steering* or the so-called *dynamical reorientation* of adsorbing molecules, favouring the adsorption and dissociation of the *helicopter* H_2 molecules. Based on PES, also *rotational-translational energy transfer* and *vibrational excitation accompanied by rotational cooling*, as well as *rotational excitation accompanied by vibrational de-excitation*, can be deduced [57]. Because of the steering effect, fast desorbing H_2 molecules will behave in the manner of a helicopter, and the slow ones, a cartwheel. The energy transfer and its relation to the total kinetic and vibrational energy are very complex. While the mean kinetic energy of desorbing molecules in the ground vibrational state first increases with rotational excitation and then decreases, this effect is not so very pronounced for the first excited vibrational state (see Figs. 3 and 4 in Ref. [42]).

In the above treatments, the surface does not show the detailed structure in both adsorption and desorption dynamics and behaves as a flat plane. Unfortunately, hydrogen desorption hardly shows the surface structure dependence, probably because the atomic distance in H_2 is too short compared with the separation of adsorption sites. Thus, for example, the structure of the site where the reaction event really takes place has disappeared in the *distribution function* of the sticking probability [42,58]. In fact, no successful interpretation of internal energy analysis in the angle-resolved form has been found for desorbing hydrogen molecules. On the other hand, the above discussion on the hydrogen molecule may not be valid for heavier molecules, such as N_2 or CO_2, because their molecular masses are comparable to the masses of the surface metal atoms and, therefore, the coupling of molecular vibrations with the phonon vibrations should not be neglected.

2.2 Site-sensitive desorption dynamics

In the third generation, investigations will aim at finding the dependence of the desorption dynamics on surface structures at the atomic level, as well as the reaction mechanism of the desorption process. The relation of desorption dynamics to the detailed site structure will be provided through analysis of the translational and internal energy of desorbing molecules as a function of the

desorption angle as well as the surface crystal azimuth. At present, no report has been found on the dependence of the internal energy on the desorption angle.

Nevertheless, the spatial and velocity distributions have already been successfully used to differentiate reaction mechanisms and to identify reaction sites. In fact, the spatial distribution of desorbing products from a surface reaction has already been found to depend on both the surface structure and on the reaction mechanism for reactive CO_2 and N_2 desorption. In the last two decades, the dynamics of CO_2 desorption have been intensively studied in CO oxidation on a number of metals under different experimental conditions [15,17,18]. The results have thrown light on many details of the surface processes and have helped to steadily improve the knowledge of the reaction mechanism. However, this molecule is not suitable for state-resolved measurements because of the lack of sensitive methods. N_2 is more promising in this respect because the highly sensitive REMPI can be applied [31].

In this paper, attention is focused on the dynamics of nitrogen desorption in NO and N_2O decomposition and in N_2 recombination on transition metal surfaces. This subject is not only requisite in developing new experiments and a theoretical approach for desorption dynamics in the next generation but also useful for the practical improvement of catalysts.

3.   NO DECOMPOSITION

Adsorption and dissociation of NO on transition metals have been intensively studied, and the results of numerous studies on metals were satisfactorily reviewed in two stages, first, in 1984 by Lambert and Bridge [59] and, recently, in 2000, by Brown and King [60]. Knowledge gained on well-defined surfaces of single crystals is a good fundamental level to be used in understanding the complicated systems of real catalysts.

3.1 Decomposition

Adsorption of NO on some transition metals is molecular, while, on the others, it is accompanied or followed by dissociation. Based on the heat of adsorption [61,62], a border was drawn between the two groups of metals (see Fig. 14 in Ref. [63]). A non-dissociative adsorption is expected on Cu, Pd, Ag, Pt, and Au, while the elements to their left in the periodic table, e.g., Ni, Rh, Ru, and Ir, would cause dissociation. Fixing this border was too simple, and dissociation is now well known to depend on the crystal plane and the presence of surface irregularities and defects, surface temperature, and surface coverage [5,60].

NO is not dissociated by Pt(111), Pt(110) or Pt(100) at room temperature, but it is on the (1×1) metastable phase of Pt(100) [60]. Structures of low index fcc planes and stepped fcc surfaces are shown in Fig. 1. On the other hand, Pt(112) = [(S)3(111)×(001)] does not dissociate NO at room temperature [64], but it does at around 480 K [65]. Similarly, NO is partly dissociated on Pd(100) at room temperature [66] but adsorbs molecularly on Pd(111) [66,67,68,69,70,71], from where it desorbs intact in the temperature range of 510-540 K. Stepped Pd(112) [70,71,72] and Pd(331) [73] surfaces are also very active in NO dissociation. On Pd(110) [74], NO adsorbs molecularly below 440 K and undergoes competing desorption and dissociation above this temperature.

3.2 Structure change

NO is molecularly adsorbed at room temperature with the N atom attached to the Pd(110) surface and the N-O axis being perpendicular to the surface [75,76,77]. The adsorption of NO itself causes a reconstruction of this surface (see schematic phase diagram in Fig. 2 of Ref. [78]). At a temperature below 200 K, the reconstruction scheme is simple. At low exposure, NO is adsorbed to two-fold bridge sites and forms a (2×1) overlayer over the (1×1) unreconstructed surface. Above the 0.5 monolayer (ML), both bridge sites and on-top sites become populated. Beyond about 0.8 ML, a metastable (2×2)p1g1 overlayer is observed, arising from $(NO)_2$ dimers formed on the (1×2) reconstructed surface. On the other hand, at 300 K, NO(a) induces a (1×3) missing-row reconstruction of the surface, and, at 0.5 ML, NO-covered (2×1) overlayer lifts the reconstruction into the (1×1) form. Above this coverage, the surface reconstructs into a (1×3) missing-row structure.

The reconstruction becomes complex when NO dissociates. Typical examples have been reported on Rh(110) [79]. On this surface, NO dissociates at room temperature and forms separate domains of (1×2)O and (2×1)N. Their periodicity is oriented perpendicularly to each other. At high coverage, the growing (1×2)O islands displace (2×1)N domains, yielding a mixed c(2×2)N+O layer on a (1×2) reconstructed surface. This change in the surface structure suggests the difficulty in applying simple analysis of the kinetics data to derive the reaction pathway.

3.3 Decomposition pathway

The reaction mechanism of the NO decomposition above 440 K on Pd(110) has been deduced from thermal desorption and molecular beam experiments [74]. A set of elementary steps was proposed, being comprised of: (i) NO adsorption, desorption, and dissociation,

(ii) N_2O formation, desorption, and dissociation, (iii) oxygen and nitrogen recombination, and desorption, and (iv) oxygen incorporation into the bulk. Nitrogen desorption was discussed as resulting from two competing processes, i.e., (i) nitrogen recombination as $2N(a) \rightarrow N_2(g)$ and (ii) N_2O dissociation as $N_2O(a) \rightarrow N_2(g) + O(a)$. A similar mechanism was also proposed on Pt(100) and stepped Pt surfaces, where the recombinative N(a) desorption was believed to proceed quickly, although no successful report on the dynamics of the $2N(a) \rightarrow N_2(g)$ process has been found on platinum surfaces [80,81]. On the other hand, on rhodium surfaces, N(a) is highly accumulated during NO dissociation, and N_2 desorbs concomitantly with N_2O above 350 K. Rh(100) is active for NO dissociation, however, the steady-state activity is not high because the adsorbed nitrogen can hardly desorb. Adsorbed nitrogen atoms play an important role in the catalytic reduction of NO [82,83]. Thus, although the turnover numbers for the NO + CO process are similar on Rh(111) and Rh(110), the N_2O *versus* N_2 selectivity is much lower on Rh(110) than on Rh(111) as a consequence of different surface coverage of the adsorbed N and NO on the two surfaces [84]. Because dissociation of NO is easier on Rh(110) than on Rh(111), the steady-state coverage of N(a) is higher on Rh(110) than on Rh(111). Higher N(a) coverage favours N atom recombination (formation of N_2) relative to NO + N reaction (formation of N_2O).

There are several limitations in applying simple analysis to kinetics to uniquely derive the reaction pathway of nitrogen removal during NO decomposition. First, the reaction mechanism is not simple. The rate-determining step is not always the removal of N(a). Rather, the dissociation of NO mostly controls the overall reaction rate. The reactivity of N(a) toward NO(a) is highly influenced by the coverage as well as the surface structure and nature of the metal [85,86]. Furthermore, it is difficult to characterize the formation and decomposition of $N_2O(a)$. The lifetime of this species must be very short in the course of catalyzed NO decomposition above 450 K because of the small heat of adsorption of N_2O. Decomposition of N_2O also strongly depends on the surface structure and nature of the metal, as discussed in Section 5.

As already stressed above, analysis of spatial and velocity distributions of desorbing product molecules is a powerful tool to cope with the dynamics of key processes involved in product formation and emission [15]. It works well even when the desorption of the product is neither the rate-determining step nor related to a stable intermediate. In the next section, the focus is on the results of the dynamics research for the following nitrogen removal processes: $2N(a) \rightarrow N_2(g)$ (Sections from 4.1 to 4.4), $NO(a) + O(a) \rightarrow NO_2(a)$

$\rightarrow$ NO$^-_3$(a) $\rightarrow$ N$_2$(g) (Section 4.5), and N(a) + NO(a) $\rightarrow$ N$_2$O(a) $\rightarrow$ N$_2$(g) + O(a) (Section 4.6).

4.   REMOVAL OF SURFACE-NITROGEN

4.1 Recombination: 2N(a) $\rightarrow$ N$_2$(g)

N$_2$ is isoelectronic with CO (see Fig. 2) and therefore its bonding to a transition metal is similar to that of CO. It is based on an interplay between electronic donation from the N$_2$ σ molecular orbitals to the metal d$_\sigma$ orbitals and back-donation from the metal d$_\pi$ orbitals to the N$_2$ π* molecular unoccupied anti-bonding orbitals [87]. In contrast to CO, the N$_2$ σ orbitals, i.e., $2\sigma_u$ and $3\sigma_g$, are equally shared by the two N atoms, and the resulting donor bond is weak. In addition, the back-donation is weaker than in the CO case because, at CO, the amplitude of the LUMO (2π) is larger on the C atom [88]. This results in a weak bond between nitrogen and transition metal surfaces. Adsorption depends on the nature of the metal as well as on its surface structure. Based on the heats of adsorption [61,62], a rough guide was made for whether or not nitrogen will be dissociated on a metal (see Fig. 14 in Ref. [63]). However the heat of adsorption is not the only factor determining the N$_2$ dissociation; hence, the real situation is much more complex. Thus, on Pt(111), nitrogen is only physisorbed [89]. On Pd(111) [90] and Ni(111) [91], physisorbed and chemisorbed molecular nitrogen coexist, while, on more open surfaces of Pd(110) [92], Ni(110) [93], and Pd(100) [94], only chemisorption has been observed. The interaction of nitrogen with metals has been well described in three review papers [95,96,97]. Generally, there are three basic states of the chemisorbed nitrogen: (i) in the α state, N$_2$ molecules lie on the surface and are strongly bound with both N atoms, (ii) the β state represents the adsorbed N atoms, and (iii) the γ state denotes weakly adsorbed N$_2$ molecules in the upright position. The α state is a precursor for the β state, i.e., dissociation.

Here, the interest is limited to the dynamics of nitrogen recombinative desorption from transition metals, i.e., its removal from the surface. It is the reverse process of the dissociative adsorption of nitrogen. We can classify the metal surfaces into two groups with respect to N$_2$ dissociation, active and inactive. On the metals of the first group, desorption can be induced after simple N$_2$ exposure yielding dissociation. All the noble metals belong to the second group. Some of them are used in real NO$_X$ catalytic treatments. Because of the very small dissociation probabilities, surface-nitrogen atoms are prepared in several ways, e.g., through (i) NO, NH$_3$, or N$_2$H$_2$ dissociation, (ii) N$_2$ excitation by electron

bombardments, or (iii) nitrogen atom beams. It should be noted that the behaviour of nitrogen atoms depends on the procedure of their preparation.

4.2   Active metals for N_2 dissociation (W, Fe, Ru)

These metals are not useful in NO_X treatments because of the difficulty of oxygen removal.   On tungsten, N_2 dissociative adsorption may proceed *via* two channels, *activated* and *precursor-mediated* [98,99,100,101].   On W(100), the precursor-mediated mechanism dominates at kinetic energies of an incident beam below 0.45 eV, while it is of minor importance on W(110). Angle-resolved analysis of nitrogen emission showed a simple cosine distribution on W(310), while desorption collimated sharply along the surface normal on W(110), approximated by $\cos^{(3-4)}\theta$ [98].

On polycrystalline Fe, the first measurements of the internal energy of desorbing N_2 were performed by the Bernasek's group [102,103]. Vibrational and rotational energy of desorbing N_2 was determined by using electron-beam-induced fluorescence.   On a clean Fe surface at the surface temperature between 1086 K and 1390 K, the vibrational temperature was slightly higher than the surface temperature, while on the surfaces covered by sulfur, a vibrational temperature significantly higher than the surface temperature was found. On the other hand, the rotational temperature was about 400 K at the surface temperature between 1086 K and 1239 K, irrespective of the sulfur coverage. This low rotational energy and its independence on the surface composition were explained by steric constraints on the recombination process. Dissociative adsorption of N_2 incident to the Fe surface was shown to be highly dependent on the initial kinetic energy, which does not make a significant contribution to directly promote the dissociation process but rather facilitates overcoming the potential barrier toward the precursor state [104]. Dissociation is also promoted by vibrational energy, although it is only half as effective as kinetic energy [32].

Ruthenium catalysts now increase their share in the ammonia synthesis instead of alumina-supported iron catalysts, but this metal is not used for NO_X treatments.   Matsushima first studied the dynamics of recombinative desorption of nitrogen on Ru(001) [14] by AR-TDS (angle-resolved thermal desorption spectroscopy). Because of the very low sticking probability for nitrogen dissociative adsorption (below 1×10^{-8}), he used an Ar^+ gun to atomize N_2 [105] and produce N atoms on the surface. Isotope experiments confirmed that desorption was purely a result of recombination reaction, $2N(a) \rightarrow N_2(g)$. Angular distribution of desorbing N_2 was described as

$\cos^n\theta$, with the n value being 7 ± 3.

In a recent study, Murphy *et al.* investigated the dynamics of recombination of N atoms left on a Ru(001) surface after NH_3 cracking [106]. In addition to confirming the translational excitation of desorbing N_2 molecules (the mean translational energy 0.62 eV), they also found an inverse vibrational population (1.4 for population ratio $v = 1$ *versus* $v = 0$) and subthermal rotational energy (rotational temperature 630 K at the surface temperature of 900 K). Their DFT calculations support their observation that N_2 vibration is excited in preference to translation. This was explained as resulting from the initial repulsion being more pronounced in the N-N coordinate of the transition state than in the N_2-surface coordinate, while rotational cooling probably reflects steric constraints on the geometry of the transition state and thus inhibition of adsorption-desorption by rotation. A preferential excitation of vibration was also observed and supported by DFT calculations in laser-assisted associative desorption of N_2 from the Ru(0001) surface [107,108]. Only about one third of the energy necessary to surmount the barrier was transferred into translation and internal degrees of freedom, all the rest was released to the surface [109].

4.3 Noble metals (Pt, Cu, Ag, Pd, Rh)

Platinum group metals are used for the three-way catalysts because most of these metals are able to dissociate NO and the resultant O(a) and N(a) can be removed in chemical reactions under moderate conditions. However, study of the dynamics of N(a) removal processes is limited, as these metals cannot dissociate the strong N-N bond in N_2 and it is then difficult to accumulate *pure* N(a) in a significant amount. Therefore, it should be noted that the experimental conditions used to study the dynamics are in most cases far from the conditions under which N_2 dissociation takes place. For example, in recent nitrogen atom beam (from a microwave discharge cavity) experiments, adsorbed nitrogen atoms were highly accumulated on noble metals; therefore, they can be used to study desorption dynamics [110,111].

There has been no report on the dynamics of the recombinative desorption of N(a) on flat platinum surfaces. During NO_X decomposition on Pt(100), the process $2N(a) \rightarrow N_2(g)$ was kinetically treated to take place quickly [112]. N_2 itself hardly dissociates on Pt(111), Pt(335), and Pt(112) at 300 K [113]. Adsorption at 90 K produces α (molecular) and β (atomic) nitrogen adspecies [114].

Adsorption of atomic nitrogen to copper causes severe surface

reconstructions [115,116,117,118,119]. In a study of nitrogen recombination dynamics on Cu(111), the surface at 700 K (slightly above the desorption temperature of N_2 recombination) showed an ordered Cu(100)-c(2×2) structure below 0.01 ML [110,111]. The translational energy as well as vibrational and rotational energy of desorbing N_2 molecules was measured by applying TOF (time-of-flight) and REMPI techniques, respectively. Desorbing molecules were translationally and vibrationally excited, with 4.2 eV translational excitation perpendicular to the surface and a vibrational temperature of 5100 K, the $v = 1$ mode being 75 times more popupated than expected from thermal population. Their rotational temperature slightly exceeded the surface temperature. To analyze the angular distribution of desorbing N_2, a Cu(100)-c(2×2)N overlayer of 0.42 ML was prepared and flashed. Desorption collimated sharply along the surface normal and was approximated by $\cos^n\theta$, with an n value of 28 ± 1. As for the hydrogen adsorption and recombination on Cu described in Section 2, vibrational and rotational energy obviously plays an important role in the adsorption and recombination of surface-nitrogen on copper.

On Ag(111) [120], the desorption dynamics of nitrogen recombination was very different from that on Cu(111). In the thermal desorption spectra of desorbing N_2, two peaks appeared at 400 K and 440 K. Desorption was sharply focused along the surface normal, described as $\cos^n\theta$, with an n value of 75 ± 5. By applying the one-dimensional barrier model [26,27], the authors estimated a translational energy of 1.3 eV. Although this translational energy was lower than that on Cu (4.2 eV), the desorption from Ag was more sharply collimated. Since the authors were not able to measure the desorption signals of the $v = 0$ and $v = 1$ vibrational states by REMPI, they assumed the higher vibrational and rotational states to be populated. By an analogy with the results on Ru(0001) [121], they proposed this excitation to be caused by the formation of nascent N_2 with an extended N-N bond.

On a Pd(110) surface sputtered with N_2^+ and N^+ ions with an incident energy of 100 eV and heated, Ikai and Tanaka reported that, in a plane in the [001] direction, the angular distribution of two N_2 peaks at 460 K and 540 K was described by $\cos^{(6-7)}\theta$ [122]. By applying ^{15}N isotope labeling, they confirmed that this N_2 desorption was due to surface-nitrogen recombination [123].

Nitrogen desorption phenomena on Rh surfaces are complicated and not fully understood, although the interaction of N with Rh has been intensively investigated, this metal being the most important component of the three-way catalysts [97]. When nitrogen atom beams were introduced onto Rh(111) [124], two maxima were

observed in the subsequent thermal desorption, one at 450 K, and the other, in the range of 561-712 K. The kinetics of N(a) recombination on Rh(111) were also studied by applying electron beam dissociation of NO and analyzing desorption spectra at various coverages [125,126]. Three alternative states of N adatoms were proposed as resulting from: (i) three different surface phases, (ii) three different ordered structures of N, or (iii) three different interactions of N-N with the near neighbors.

4.4 N_2 desorption in NO decomposition

Desorption dynamics of N_2 from NO decomposition is sometimes very different from that for $2N(a) \rightarrow N_2(g)$ because the N(a) removal does not always proceed *via* the recombination process. Characteristic examples were found on Pd(110) and are presented below.

4.4.1 Pd(110)

Peculiar desorption of N_2 in the thermal decomposition of NO was first noticed by Ikai and Tanaka on Pd(110) [127,128,122]. The emission of N_2 was maximized at an angle θ of about 37° off-normal to the surface in the [001] direction. It was approximated by $\cos^{46}(\theta$ - 37°) in the [001] direction and by $\cos^{4.2}\theta$ in the [$1\bar{1}0$] direction. They argued that the inclined desorption was caused by a direct collision of two NO admolecules and not through $N_2O(a)$ dissociation.

AR-TDS spectra of desorbing N_2, N_2O, and NO, which were later observed by Ohno *et al.* [11] using a more sophisticated apparatus after a clean Pd(110) was exposed to NO at around 350 K and then heated, are shown in Fig. 3. Desorption of N_2, NO, and N_2O commonly peaked at around 490 K, suggesting that NO(a) dissociation was rate-limiting. The N_2 signal at $\theta = \pm41°$ was more intense than that in the normal direction. The analysis of the angular distribution showed that N_2 desorption in the [001] direction was maximized at $\theta = \pm41°$ and can be approximated by $\cos^{28}(\theta + 41°)$ + $\cos^{28}(\theta - 41°)$ (Fig. 4a). Desorption of NO and N_2O showed a simple cosine distribution. These angular distributions indicate that N_2 is desorbed with an excess translational energy, while NO and N_2O are accommodated to the surface before being desorbed. This was confirmed by velocity measurements. The velocity distribution of N_2 measured at $\theta = 41°$ was deconvoluted into two hyperthermal components with translational temperature [129] $T_{<E>} = <E>/2k$ of 2700 K and 1300 K (Fig. 4b). On the other hand, the velocity

distributions of NO and N_2O follow the *Maxwellian* distribution at 490 K.

Because of the similarity in the dynamic characteristics of N_2 in the thermal decomposition of NO shown here and N_2O on Pd(110) discussed later (see Sections 5.2 and 5.3), $N_2O(a)$ was proposed as an intermediate in NO decomposition. NO(a) is partly desorbed and partly dissociated into N(a) and O(a). The interaction between NO(a) and N(a) results into the formation of $N_2O(a)$, which may desorb or dissociate into $N_2(g)$ (or $N_2(a)$) and O(a).

4.4.2 Rh(111)

N_2 desorption dynamics on Rh(111) was studied in the temperature range of 700-1000 K. The impinging continuous beams of NO and H_2 yielded N(a) below 0.05 ML [130]. From the angular distribution of desorbing N_2, two components were deduced, one with a simple cosine distribution, and the other, sharply collimating along the surface normal in a $\cos^n \theta$ form, with an n value of 25 ± 5. The angular distribution was insensitive to the surface temperature. Two components were also identified in velocity measurements. One showed that the translational temperature was about six times higher than the surface temperature, and the other showed that it was about two times higher. Three possibilities were discussed: (i) N_2 is produced by two different reactions: $2N(a) \rightarrow N_2(g)$ and $N(a) + NO(a) \rightarrow N_2(g) + O(a)$, (ii) N adatoms to produce N_2 come from two different environments: individual adsorption sites or N islands, (iii) N_2 is in two vibrational states as a consequence of the elongated N-N bond in the transition state. By using ^{15}N isotopic labeling of NO, Zaera *et al.* have discussed the possibility of the N_2O intermediate in NO reduction by CO [10].

4.4.3 Stepped surfaces

In thermal NO decomposition on Pd(211) = [(S)3(111)×(100)], N_2 desorption was also accompanied with N_2O below 600 K [123]. Desorption of N_2 collimated at an off-normal angle in the direction down the steps, being approximated by $\cos^{12}(\theta + 26^{\circ})$. N_2 was suggested to be produced on the (100) steps. For a few fcc stepped surfaces relevant for this work, the microfacet normals and the angles they form against the global surface normals are shown in Fig. 5.

Desorption of N_2 was also studied on Rh(533) = [(S)4(111)×(100)] [131]. N_2 showed a sharp peak at 450 K and two broad peaks between 500 K and 600 K after the crystal was exposed

to NO at 300 K and then heated. The first peak sharply collimated at $\theta = -15°$ in the direction perpendicular to the steps. The 500-600 K desorption showed a broad distribution with a maximum at $\theta = -15°$. This clearly indicates that N_2 desorbs neither along the normal of the (111) terrace nor along the (100) step normal. This peculiar N_2 desorption was proposed to originate from a pre-desorption precursor located at the border between the terraces and steps.

An alternative explanation could be based on the surface reconstruction or the dissociation of N_2O properly oriented on the surface, as discussed in Sections 5 and 8, but was not considered by the authors.

4.5 NO$_2$ oxidation and reduction

4.5.1 Adsorption and dissociation of NO$_2$

NO_2 has a very rich chemistry on metals. For example, on a clean Rh(111) surface, it dissociates below 150 K, producing NO(a) and O(a). Most NO(a) further dissociates into N(a) and O(a) at 300-400 K [132]. The adsorbed O atoms readily diffuse into the subsurface from where they segregate to the surface and desorb above 650 K [133]. The initial dissociation of NO_2 on Ru(001) is suppressed by NO and O adspecies left on the surface from dissociation. Upon heating to 300 K, the NO(a) dissociates into N(a) and O(a). Increasing NO_2 exposure leads first to the formation of a NO_2 monolayer and then to the production of $(NO)_2$ dimers [134].

On Pd(111), NO_2 chemisorbs molecularly below 180 K and dissociates above 530 K [135,69]. On Pt(111), adsorption is molecular below 100 K but dissociative above 285 K [136,137]. If an Ag surface pre-covered by oxygen is exposed to the NO_2, nitrate species NO^-_3(a), is produced [138,139,140]. If such a surface is heated above 475 K, NO^-_3(a) is decomposed, and NO(g) desorption and N(a) accumulation are observed [140]. The latter recombines with O(a) to produce NO(g). Formation of NO^-_3 was also observed on Zn [141]. Compared to the metals mentioned above, Mo has the highest ability to cleave the N-O bond. On Mo(110) [142], dissociation of NO_2(a) into NO(a) and O(a) was observed at 100-150 K, followed by dissociation of NO(a) into N(a) and O(a) at 250-350 K. Dosing of NO_2 at 300 K results in direct production of desorbing NO(g) and the formation of a surface layer of MoO_2 by O(a).

4.5.2 Controlled catalytic cycles

A well-controlled interplay between NO_2 oxidation into nitrate and NO_2 reduction into NO and O, followed by NO dissociation into N(a) and O(a), is the essential point of the reaction mechanism of nitrogen removal with the new-concept three-way catalyst, the so called 'NO$_X$ storage-reduction catalyst' (NSR), installed in cars with lean-burn engines [143]. To prepare the catalyst, the alumina support is impregnated by precious metals, various alkaline and alkaline earth metals (mainly Ba), and rare earth metal oxides [144,145,146,147,148]. During the oxidizing step of the operational regime of the catalyst, NO is oxidized on the precious metal into NO_2, which then recombines with NO to produce nitrate. During the reducing step, nitrate is decomposed into NO by reducing agents (e.g., CO, hydrocarbons) activated on the precious metal. The emitted NO is reduced to N_2 on the precious metal by reducing agents. N_2 is released, and the nitrogen removal scheme is completed [144].

The desorption dynamics of NO have been studied in NO_2 decomposition under reducing and oxidizing conditions on Rh(111) in the temperature range between 500 and 1000 K [149]. In the reducing regime, the surface was exposed to a constant flow of NO_2 and H_2. Desorption of NO showed a bimodal distribution at 600 K, approximated by $0.43 \cos^{2.8}\theta + 0.57 \cos\theta$, while it was a simple cosine form at 1000 K. At 800 K, the mean translational energy of NO was 315 meV, as compared with 138 meV which was equivalent to the surface temperature. The oxidizing conditions were achieved by switching off the H_2 beam and allowing oxygen, released in NO_2 dissociation, to accumulate on the surface. Under these conditions, the angular distribution of NO desorption was cosine, slightly collimating along the surface normal, and its translational temperature was practically equal to the surface temperature. Thus, changing the experimental conditions from reducing to oxidizing obviously switches the channel for NO production, and, hence, the dynamics of the NO produced. Here, oxygen was explained to affect the interaction between NO_2 and the surface and not the geometry of the adsorbed NO_2, as proposed on other transition metals.

No structure information on the reaction can be deduced from desorbing NO because it is desorbed after being accommodated to the surface [15].

4.6   N(a) + NO(a) → N₂O(a) → N₂(g) + O(a)

This reaction is part of the complex reaction mechanism on the three-way catalyst. The N_2O formation reaction was extensively studied on Pt(335) = [(S)4(111)×(001)] [150]. NO admolecules from

the (111) terraces were confirmed to be most reactive towards N(a), while, among the N(a) species, most active were those produced by NO dissociation on steps. Interestingly, N adatoms produced on terraces were more easily recombined than those produced on steps. However, no evidence was found for the N_2O dissociation process on platinum surfaces.

The contribution of the N_2O intermediate in the decomposition pathway in NO treatments was first proposed on rhodium because of the high concomitant N_2O formation [151]. The reaction N(a) + NO(a) $\rightarrow$ N_2(g) + O(a) was first proposed on Rh(111) [152,153,154,155]. No direct evidence has been found for the contribution of this process, although the N_2O decomposition can take place even around 100 K on Rh(110). The dynamics of the reaction N(a) + NO(a) $\rightarrow$ N_2O(a) $\rightarrow$ N_2(g) + O(a) have been studied only indirectly through the thermal decomposition of NO on Pd(110) by our group [11,156]. This could be done because the rate-determining step is NO(a) dissociation and not N_2O(a) dissociation.

Because, as seen later in the text, N_2O plays a crucial role in the inclined desorption of N_2 in the NO and N_2O decomposition and the NO + CO reaction, the geometry of N_2O(a) and its orientation on Pd(110) are discussed in detail in Section 8 on the basis of DFT calculations.

5. N_2O DECOMPOSITION

N_2O decomposition is sensitive to the kind and surface structure of a metal. In fact, N_2O(a) desorbs at 90-100 K without dissociation on Pt(111) [157], Ir(111) [158], Ni(111) [159], or Ag(111) [160], but it dissociates at about 100 K on Ru(001), W(110) [161], Cu(110) [162], and Ni(557) [163]. Incident N_2O was decomposed on Ni(110) and Ni(100) below 200 K [164,165] but not on Rh(111) [166]. On Pd(110), Rh(110), and Ir(110), the dissociation of N_2O(a) starts at around 100 K and is completed at around 160 K [167]. During this dissociation, N_2 is emitted, and oxygen atoms are left on the surface. AR-TDS combined with TOF is the best method to study the desorption dynamics of this N_2. Using this method, Ohno *et al.* found the peculiar angular and velocity distributions of desorbing N_2 on Pd(110) [11].

5.1 TDS-TOF

Their experiments were performed in an ultra-high vacuum apparatus (UHV) consisting of three chambers pumped separately,

i.e., a reaction chamber, a chopper house, and an analyzer. The principle behind the apparatus is schematically shown in Fig. 6 [168]. A good angle-resolved signal can be attained with a high pumping rate of the reaction chamber and the chopper house [169]. The reaction chamber was equipped with LEED-AES (low electron energy diffraction - Auger electron spectroscopy) optics, an Ar^+ gun, a gas handling system, a sample manipulator and a quadrupole mass spectrometer (QMS) for angle-integrated (AI) signals of desorbing gases. The chopper house faced the reaction chamber with a 1.0 mm × 6.0 mm slit and contained a cross-correlation chopper blade with 1.0 mm × 6.0 mm slots distributed pseudo-randomly in a double sequence of 255 slots each (see the inset in Fig. 6). The analyzer was equipped with another QMS operating in a pulse-counting mode.

A disc-shaped sample crystal that was 1 mm thick and had a diameter of 10 mm was fixed on an L-shaped manipulator whose rotation defined the angle between the sample surface normal and the analyzer axis (the line-of-sight position of the QMS). Molecules desorbing from the sample surface and passing the two slits could be detected by the QMS in the analyzer, yielding angle-resolved (AR) signals. For velocity measurements, the flow of molecules was modulated by the chopper after the first slit, and their arrival times to the ionizer of the QMS in the analyzer were recorded to obtain TOF spectra [129].

5.2 Pd(110)

Ohno *et al.* first examined the angular and velocity distributions of N_2 and N_2O in thermal decomposition of $N_2O(a)$ [11,156,170]. Since their work was limited above 130 K, Horino *et al.* extended measurements with exposing N_2O at about 95 K [171,172,13]. The reported AI and AR thermal desorption spectra of N_2 are shown in Fig. 7. We can see large differences in the TDS (thermal desorption spectroscopy) spectrum shape between the AI and AR forms. The latter was sensitive to the desorption angle. The AR spectrum was deconvoluted into four *Gaussian*-distribution peaks (presented by dotted lines in Fig. 7b and 7c). They were named as β_1-N_2 at 150 K, β_2-N_2 at 134 K, β_3-N_2 at 123 K and β_4-N_2 at 110 K. These peak temperatures were insensitive to the N_2O exposure. The β_2-N_2 emission followed a simple cosine form in the plane in the [$1\bar{1}0$] direction (Fig. 8a). In the plane perpendicular to it (i.e., in the [001] direction), two maxima due to β_1-N_2 were additionally observed in this β_2-N_2 emission when N_2O was exposed at 130 K. These distributions are drawn in three dimensions in Fig. 8b. On the other hand, the other N_2 peaks were bi-directional, sharply collimating at an off-normal angle in the normally directed plane in the [001] direction. These distributions were approximated as follows (Fig.

9):

β_1-N$_2$ at $\Theta_{N_2O} = 1.0$: $\qquad \cos^{50}(\theta + 43^\circ) + \cos^{50}(\theta - 43^\circ)$

β_3-N$_2$ at $\Theta_{N_2O} = 0.2$: $\qquad \cos^{50}(\theta + 43^\circ) + \cos^{50}(\theta - 43^\circ)$
$\qquad$ at $\Theta_{N_2O} = 1.0$: $\qquad \cos^{30}(\theta + 43^\circ) + \cos^{30}(\theta - 43^\circ)$

β_4-N$_2$ at $\Theta_{N_2O} = 0.03$: $\qquad \cos^{28}(\theta + 50^\circ) + \cos^{28}(\theta - 50^\circ)$
$\qquad$ at $\Theta_{N_2O} = 0.2$: $\qquad \cos^{50}(\theta + 44^\circ) + \cos^{50}(\theta - 44^\circ)$

where Θ_{N_2O} is the relative N$_2$O coverage. The observed distributions are commonly characteristic of sharp and highly inclined desorption. These desorption peaks were mostly suppressed in the plane along the [$1\bar{1}0$] direction. On the other hand, the distribution of N$_2$O desorption had a simple cosine form.

The β_2-N$_2$ component was proposed to be produced from N$_2$(a) trapped in the reaction N$_2$O(a) $\rightarrow$ N$_2$(a) + O(a) because its translational temperature was equal to the surface temperature [170]. Furthermore, the peak temperature was consistent with N$_2$ desorption from a clean Pd(110) surface [92]. On the other hand, β_1-N$_2$ possesses a high kinetic energy [11,156,170]. In order to avoid a large contribution of β_2-N$_2$, velocity measurements of β_1-N$_2$ were performed at 152 K in TDS procedures after the surface was exposed to 0.20 L (1 *Langmuir* equals to 133 µPas) of N$_2$O at 130 K. Figure 10 shows the resultant velocity distribution of β_1-N$_2$ obtained at $\theta = -43^\circ$. After subtracting the background from the experimental distribution, it was deconvoluted into two components, each described by a modified *Maxwellian* form [129,15]:

$$ f(v)dv \quad \propto \quad v^3 \exp\left(-\frac{(v - v_0)^2}{\alpha^2}\right)dv $$

in which v and v_0 are the velocity and stream velocity, respectively, and α is defined through the width parameter $T_W = m\alpha^2/2k$, m being the mass of a molecule and k, the *Boltzmann* constant. Both components are hyperthermal. Their translational temperatures (580 K and 1930 K) were lower than those of the N$_2$ formed in NO decomposition (1300 K and 2700 K, see Section 4.4.1) because the surface temperature here was about 340 K lower.

Sharply collimated β_3-N$_2$ and β_4-N$_2$ are expected to be

translationally excited in analogy with β_1-N_2 [15]. These three N_2 components were proposed to be produced in the $N_2O(a) \rightarrow N_2(g) + O(a)$ reaction, in which N_2 immediately desorbs before dissipating its kinetic energy. The decomposition of $N_2O(a)$ starts around 100 K when the surface is free of O(a), yielding β_4-N_2 and probably $N_2(a)$, which desorbs as β_2-N_2 at a higher temperature. A steadily increasing accumulation of O(a) influences the formation of β_3-N_2 and β_1-N_2.

5.3 Inclined desorption

The repulsive desorption in thermal reactions reported so far has been generally explained by the *Pauli* repulsion on the product molecules formed in close proximity to the surface [15]. In fact, we have shown (Sections 4.2, 4.3, and 4.4) that the desorption of N_2 produced by recombination of N(a) sharply collimated along the surface normal, except for the results on Rh(335) (Section 4.4.3), where N_2 might be desorbed *via* an N_2O decomposition process. The inclined desorption on Pd(110) might then result from N_2 molecules formed on the reconstructed patches of the surface, whose local normal declines from the (110) global surface normal [173]. The surface is reconstructed into a missing-row structure and is stabilized by a c(2×4)O overlayer if it is exposed to oxygen at room temperature. However, β_4-N_2 is formed on an oxygen-free surface at about 100 K, and no such reconstruction is expected. Furthermore, the collimation angle shifts to 65-70° on Ir(110) and Rh(110), as will be shown in Sections 5.4 and 5.5, respectively. This angle is too large compared with the declining angle of the normals of the terraces on the missing-row structure. Therefore, the inclined desorption should be examined on a flat non-reconstructed (1×1) surface. A solution to this problem was found by our group by introducing an alternative mechanism based on the dissociation of $N_2O(a)$ oriented in the [001] direction, as described below [11,13,172,167].

At the moment prior to dissociation, $N_2O(a)$ is being tilted and eventually lies on the surface in the [001] direction [11]. After the N-O bond is broken, the nascent O(a) is left on the surface and is stabilized onto the nearest adsorption site. During this process, a large amount of energy is dissipated on account of the energy of the Pd-O bond formed (the bond energy of the PdO molecule is roughly 2.4 eV [174]). The nascent N_2 receives a recoil force from this high-energy O atom. An additional force acting on the nascent N_2 is assumed to originate from the *Pauli* repulsion. Combination of both forces determines the inclined and translationally excited desorption

of N_2. This interpretation based on *high-energy O atom-assisted* mechanism is reminiscent of the *hot atom* mechanism of the photo-induced desorption of oxygen on Pt(113), in which the surface-parallel momentum plays an important role in dynamic features [175,13]. This mechanism, merely based on experimental observations and chemical intuition, has been further elaborated and clarified by applying DFT calculations and is presented in Section 8.

5.4 Ir(110)

AI and AR thermal desorption spectra of N_2 on Ir(110) at two desorption angles are shown in Fig. 11 [167]. Only two peaks were successfully analyzed for the angular distribution, although four peaks could be identified after deconvolution, in the same manner as described above for Pd(110), and were named as: β_1-N_2 at 195 K, β_2-N_2 at 170 K, β_3-N_2 at 145 K, and β_4-N_2 at 120 K. The β_1-N_2 peak showed a simple cosine form, while the β_4-N_2 distribution was approximated by $\cos\theta + 1.1\cos^{15}(\theta + 65°) + 1.1\cos^{15}(\theta - 65°)$ in the [001] direction (Fig. 12). The sharp angular distribution component in β_4-N_2 suggests an excess translational energy [15]. The high-energy O atom-assisted mechanism proposed on Pd(110) predicts a larger inclined angle on Ir(110) than on Pd(110). Because the bond energy of the IrO molecule of 4.3 eV [176] is higher than that of the PdO molecule of 2.4 eV [174], the nascent O atom on Ir is 'hotter' than that on Pd, and more energy may be transferred to the nascent N_2 molecules, thus resulting in a higher collimation angle, as actually observed. It should be emphasized that the observed collimation angle of 65° is too large to be explained by N_2 desorption along the terrace normal of the missing-row structure [173], because the terrace normal of the missing-row structure declines only for about 20° from the global surface normal.

5.5 Rh(110)

The angular distribution of N_2 on Rh(110) became interesting because a large collimation angle was expected according to the high-energy O atom mechanism. As on Ir(110), this mechanism predicts highly inclined hyperthermal N_2 desorption on Rh as well, since the energy of the Rh-O bond of 4.2 eV is similar to 4.3 eV of the Ir-O bond [176].

Four desorption peaks could be identified in N_2O decomposition, as seen in the AR thermal desorption spectra in Fig. 13: β_1-N_2 at 167 K, β_2-N_2 at 145 K, β_3-N_2 at 130 K, and β_4-N_2 at 110 K. Only two N_2 desorption peaks were successfully analyzed for the angular

distributions [177,167]. The β_1-N_2 peak showed a simple cosine distribution, while the distribution of β_4-N_2 was approximated by $\cos^{15}(\theta + 70°) + \cos^{15}(\theta - 70°)$ in the [001] direction (Fig. 14). The observed collimation angle is slightly larger than that on Ir(110). This means that the dynamic characteristics of desorbing N_2 are not simply related to only the strength of the O-metal bond but are obviously influenced by other factors as well.

5.6 High-energy O atom-assisted desorption

In the previous sections, the inclined desorption of N_2 in the thermal dissociation of N_2O on the (110) surfaces of Pd, Ir, and Rh was interpreted with the high-energy O atom-assisted desorption mechanism. This interpretation was merely based on the experimental observations on one side, i.e., the normally directed N_2 desorption in $2N(a) \rightarrow N_2(g)$ recombination and the inclined N_2 desorption in N_2O dissociation, and on the analogy with the hot atom mechanism on the other side, without theoretical calculations of the desorption event. This mechanism has an advantage based on a simple consideration, namely, that the total momentum operative towards the nascent N_2 is divided into two components, one perpendicular and the other parallel to the surface plane. This simplification brought about the idea that the surface parallel momentum is mostly due to the energy released in the formation of the oxygen-metal bond and could therefore predict a larger collimation angle of N_2 desorption on Rh(110) and Ir(110) than on Pd(110). However, the energy transfer mechanism from the hot oxygen to the nascent N_2 has not been clarified yet.

According to the hot O atom-assisted desorption, the nascent N_2 is repelled by the surface along the surface normal due to the *Pauli* repulsion because the bulky N_2 molecule is formed in close proximity to the surface. However, the normally directed force in N_2O dissociation is not expected to be as large as that in the recombinative N_2 desorption because the location of the terminal N atom in $N_2O(a)$ is further away from the surface than that of the adsorbed nitrogen atom. For inclined desorption, an additional force must be operative towards the product N_2 into the inclined direction. This force is likely to come from the nascent oxygen. A higher translational energy is generally expected for molecules with sharper angular distributions, although the translational energy generally depends on the surface crystal azimuth [178,168]. The above model predicts that the translational energy on Rh(110) and Ir(110) would be higher than that on Pd(110); hence, the angular distribution on Pd(110) must be broader than that on the other two. However, the sharpness of the angular distributions was observed in the opposite

direction. This discrepancy must be directly examined by measuring the velocity distribution or further elaborated by applying DFT calculations.

6. CATALYTIC NO DECOMPOSITION

Findings reported in Section 5 on the high reactivity of clean Rh(110), Ir(110), and Pd(110) surfaces towards N_2O are important to understand the mechanism of NO decomposition because, as explained below, N_2O is an intermediate in the decomposition of NO, and its dissociation governs the desorption of N_2. However, the literature is limited as far as the interaction of N_2O with clean metal surfaces is concerned. Its decomposition on a surface is severely retarded by the product oxygen adatoms. The adsorption becomes negligible at high temperatures when oxygen can desorb because of the small heat of adsorption of N_2O. Furthermore, the fragmentation of N_2O is serious in UHV chambers as well as in electron bombardment-type mass spectrometers. These factors might obscure the chemistry of N_2O on clean metal surfaces.

In addition to the angular distribution, the velocity distributions of NO, N_2, and N_2O molecules provided information about the thermal NO decomposition. The inclined desorption of N_2 was shown to be governed by the dissociation of the N_2O intermediate produced by the NO(a) + N(a) reaction. Angle-resolved thermal desorption combined with the TOF technique is useful to characterize N_2O decomposition [11,156]. This method is also useful to differentiate the reaction pathways under steady-state conditions because the angular and velocity distributions can provide information even if the product emission is not rate-determining. The relationship of product desorption dynamics and the rate-determining step was developed by our group mostly in the model CO oxidation on platinum metals [18].

For the NO + CO reaction under steady-state conditions, only a few papers have been reported on Pd(110) [17,12,179,180,13,18]. The crystal at the desired surface temperature was exposed to a constant flow of NO and CO, and the products N_2, CO_2, and N_2O were monitored in AI and AR forms. The reaction rate was negligible below 480 K, but it abruptly reached its maximum at about 520 K and slowly decreased toward zero at 750 K. That is one indication that NO dissociation is rate-determining and that the subsequent removal processes of oxygen and nitrogen take place quickly. Even in such cases, different angular distributions of desorbing products can be seen.

The angular distribution of the N_2 emission in a plane in the [001]

direction at temperatures between 500 K and 620 K is shown in Fig. 15. It is bi-directional, sharply collimated at $\theta = \pm 41°$, and approximated by $\cos^{28}(\theta + 41°) + \cos^{28}(\theta - 41°)$, which is similar to the N_2 distribution in N_2O dissociation on Pd(110) under TDS conditions (see Section 5.2). The desorption of CO_2 (Fig. 16) is composed of a sharp component collimated along the surface normal direction and a broad cosine component, being thus represented overall by $\cos^{15}\theta + 0.30\cos\theta$ in the [001] direction (Fig. 16a) and by $\cos^3\theta + 0.30\cos\theta$ in the [1$\bar{1}$0] direction (Fig. 16b). This angular anisotropy is the same as that in CO oxidation on unreconstructed surfaces [168]. This indicates that the Pd(110) surface was not reconstructed under the steady-state conditions. Therefore, the bi-directional N_2 desorption may not be ascribed to a (1×3) missing-row surface, but it might be necessary to consider the unreconstructed plane to interpret it. Both N_2 and CO_2 angular distributions are insensitive to the surface temperature. On the other hand, N_2O desorption follows a simple cosine form.

Velocity distributions of N_2 (at $\theta = \pm 41°$), N_2O, and CO_2 are shown in Fig. 17. In Fig. 17a, the *Maxwellian* distribution at $T_S = 540$ K (dotted line) was subtracted from the observed data because it originates from the ambient N_2 molecules in the reaction chamber, reflecting from the sample surface. The resultant distribution (open circles) was deconvoluted into two components with translational temperatures of 2660 K and 1300 K. Similar hyperthermal velocity components of N_2 were also found in NO and N_2O dissociation under TDS conditions [11,156,170]. The velocity distribution of CO_2 (Fig. 17c) is similar to that in CO oxidation under steady-state conditions [181,182,183,184]. On the other hand, the velocity distribution of N_2O (Fig. 17b) obeys a *Maxwellian* form at $T_S = 540$ K.

Because the dynamic features of the N_2 desorption in the steady-state NO + CO reaction are similar to those in thermal decomposition of NO and N_2O, N_2O(a) has been accepted as a common intermediate for all the three processes. Hence, also in the NO + CO reaction, the inclined hyper-thermal desorption of N_2 has been explained by the high-energy O atom-assisted mechanism that is operative in the dissociation of the N_2O(a) precursor, which is prior to the N-O bond rupture practically lying on the surface into the [001] direction. The details of the dissociation are described in Sections 5.3 and 8.2.

7. SURFACE ALIGNED REACTIONS

The sharply directed desorption of the fragments along the ruptured bond is well known in the dissociation of molecules by photons or electrons. Such desorption can be seen clearly on solid surfaces because chemisorbed molecules are often oriented in one direction [185,186,187,188,189,17]. This suggests that reactions on solid surfaces may take place along a one-dimensional interaction path. In fact, this was first confirmed in the photo-desorption of O_2 on Ag(110), where O_2 molecules were oriented along the $[1\bar{1}0]$ direction and the photo-desorption of O_2 was split along this direction, although the normally directed component was major [190,191].

Improved experiments were later reported in the photo-desorption of oxygen from Pt(113) [175]. A clear bi-directional desorption was observed, being approximated by $\cos^{21}(\theta + 20°) + \cos^{21}(\theta - 20°)$ at $\Theta_{O_2} = 0.08$ and by $\cos^{31}(\theta + 15°) + \cos^{31}(\theta - 15°)$ at $\Theta_{O_2} = 0.11$, Θ_{O_2} being the relative oxygen coverage. With increasing Θ_{O_2}, two additional oxygen desorption components appeared, one collimating along the surface normal and the other declining from it for 45-49°. This bi-directional desorption can only be explained by the 'hot' oxygen atom collision mechanism. Upon laser irradiation, oxygen admolecules dissociate, and hot oxygen atoms are emitted along the O_2 molecular axis, aligned along step edges. When such a hot atom collides with a nearby oxygen admolecule, the molecule may be ejected from the surface in the plane along the step edge. The ejected molecule is subjected to the hot atom momentum and the *Pauli* repulsion, which, when combined, determine the collimation angle. This desorption mechanism is very similar to that for N_2 inclined emission in N_2O dissociation.

8. ADSORPTION AND DISSOCIATION OF N_2O ON THE Pd(110) SURFACE FROM FIRST PRINCIPLES

As discussed previously in this review, N_2O as an intermediate in the nitrogen removal processes plays a crucial role in the inclined desorption of N_2 in the NO decompositions and in the NO + CO reaction. Two different explanations of the inclined desorption of N_2 have been given. Haq *et al.* [173] suggested the inclination to be due to the reconstructed surface from which N_2 desorbs along the local surface normal. On the other hand, an alternative mechanism which works well with the non-reconstructed surface as well, was provided by our research team [13,172,167] (see Section 5.3). The two models can be evaluated by means of theoretical *ab initio* calculations.

In the last decade, the DFT-GGA (density functional theory within the generalized-gradient-approximation) has proved useful

and successful in calculating equilibrium structures and other properties, such as the adsorption energy as well as the activation energies along the reaction paths [63,192]. Applying this method and using the PBE (*Perdew-Burke-Ernzerhof*) energy functional [193], Kokalj *et al.* investigated possible orientations and structures of $N_2O(a)$ on the Pd(110) surface [194,195] and proposed an explanation of the inclined N_2 desorption [196]. The Pd(110) surface was modeled with the super-cell technique using the plane-wave method with ultrasoft pseudopotentials [197]. Several super-cells were used to simulate the adsorbate coverage of 0.25 and 0.5 ML.

The valence molecular orbitals (MO) of the gaseous N_2O and a plot of their eigenvalues are shown in Fig. 18. In the adsorption, 7σ, 2π, and 3π MOs are usually considered; the last two being the HOMO (highest occupied molecular orbitals) and the LUMO (lowest unoccupied molecular orbitals), respectively. The 7σ is mainly located on the terminal nitrogen atom (N_t); hence, if the N_2O-substrate interaction is dominated by a σ-bonding, the N_t-Pd interaction is likely to be preferred. The 7σ and 2π orbitals are more or less non-bonding in nature, which implies that the interaction of these orbitals with the substrate will not significantly alter the molecular bonds. On the other hand, the LUMO 3π orbitals are strongly anti-bonding, and back-donation from the substrate into 3π orbitals will result in an elongation of the molecular bonds.

8.1 Structures of the adsorbed N_2O

8.1.1 Results of calculations

Using DFT calculation, Kokalj *et al.* [194,195] have found that N_2O binds weakly to the surface in two alternative forms: either (i) tilted with the terminal N atom attached to the surface, or (ii) lying horizontally on the surface in the [001] direction (Fig. 19). In the first case, the molecular geometry remains linear upon adsorption, with almost unchanged N-N and N-O distances. The precise estimation of the tilt angle is difficult due to the flatness of the PES. In the second case, the geometry of horizontally adsorbed N_2O molecules is not linear but bent, with the O atom pointing toward the surface. The N-N and N-O distances are longer than in the tilted structure, indicating a larger charge back-donation from the substrate into the antibonding 3π molecular orbital. The adsorption of the tilted (or upright) form *via* the oxygen atom was found to be unstable.

The horizontal on-top $N_2O(a)$ oriented in the [001] direction was found to be more stable than that in the [$1\bar{1}0$] direction, the

difference roughly being 0.2 eV (see Fig. 20 for the two N_2O(a) orientations). The rest of the text will refer to the preferred [001] orientation. Table 1 summarizes the results for various super-cells representing 0.5 and 0.25 ML adsorbate coverage. Top-view and side-view snapshots of the optimized structures are shown in Fig. 19. The adsorption on the on-top sites (binding energy $E_b \in 0.36 - 0.40$ eV) is energetically favoured and the bridge sites are less stable ($E_b \in 0.18 - 0.29$ eV). The stability of the on-top tilted and on-top horizontal forms is very similar, and their energy difference (a few 10 meV) is comparable with the estimated overall theoretical accuracy.

The interaction of N_2O with the surface can be described by coupling of (i) the molecular 7σ orbital with the substrate d_σ orbitals, where the symbol d_σ stands for the linear combination of the atomic d_{z^2} and s orbitals and (ii) the molecular 2π orbitals with the d_{xz} and d_{yz} orbitals of the substrate. The substrate back-donation into the molecular anti-bonding 3π was found to be small for the horizontal form and absent for the tilted one. These features are evidenced from the plots of the density of states projected (PDOS) to the N_2O molecule and to the surface Pd atoms that interact with the N_2O molecule, shown in Fig. 21. The charge transfer between the adsorbate and the substrate, as well as the formation of a chemical bond between them, is also characterized in terms of the charge density difference, $\Delta n(\mathbf{r}) = n_{N2O/Sub}(\mathbf{r}) - [n_{N2O}(\mathbf{r}) + n_{Sub}(\mathbf{r})]$, as plotted in Fig. 22. Here, $n_{N2O/Sub}(\mathbf{r})$, $n_{Sub}(\mathbf{r})$, and $n_{N2O}(\mathbf{r})$ are the electron charge density distributions of the N_2O-on-substrate, clean substrate, and N_2O, respectively. As seen from Fig. 22, the horizontal N_2O(a) species interact with the surface not only with the terminal-nitrogen atom but also with the oxygen atom.

8.1.2 Comparison between calculated and experimental results

The above results generally agree with the experimental observations. From RAIR (reflection-absorption-infrared spectroscopy) spectra of N_2O(a) on Pd(110), Haq and Hodgson [173] suggested that N_2O is adsorbed upright with the terminal N atom attached to the surface. The lying form is inactive to this method. The results from NEXAFS (near edge X-ray absorption fine structure spectroscopy) are also consistent with the above calculations. The inclined N-N bond in N_2O(a) toward the surface plane was examined, although the definite configuration has not been obtained yet. This admolecule shows two π^* resonances and one broad σ^* resonance above the X-ray absorption edge of the nitrogen 1s state. The σ^* resonance, sensitive to the molecular orientation, was mostly

suppressed on the surface. The π^* resonances are due to the transition from the 1s state of the terminal and central nitrogen atoms to the $3\pi^*$ unoccupied state. This resonance intensity must change sharply with the X-ray incidence angle when the N-N bond is oriented only along a fixed direction. However, the observed resonance intensity was fairly insensitive to the X-ray incidence angle, as commonly observed on Pd(110) [198] as well as on the other reported surfaces, Ni(111) [159], Cu(100), and Ag(110) [199].

Two possible explanations cannot be differentiated at present. The first assumes only one adsorption form yielding a bent admolecule. In this model, the N-N bond must largely incline from the surface normal [200]. On the other hand, in the second model, two adsorption forms are assumed: one is standing, and the other is lying on the surface. The insensitive incident angle-dependence can be predicted when the two forms can easily convert into each other. In fact, there are only small energy differences between the proposed tilted and lying forms. The DFT results are consistent with the second model [194]. A bent form was also proposed from the kinetic isotope effects on polycrystalline Cu [201]. The inclined N-N bond in $N_2O(a)$ was also proposed on Pt(111) from bi-directional oxygen atom desorption collimated at $\pm40°$ off-the-surface normal in the photo-dissociation of $N_2O(a)$ at 197 nm light [202,203].

The experimental adsorption heat of 0.39 eV was obtained from the TDS peak temperature (150 K) of N_2O desorption [170], assuming the simple first-order desorption and non-activated adsorption [204] of N_2O on Pd(110). The abovementioned DFT values agree quite well with this experimental value, thus giving good support to our present picture of the N_2O adsorption.

8.2 Dissociation of $N_2O(a)$

The horizontal $N_2O(a)$ species lying on the surface in the [001] direction is a good candidate for the precursor of the $N_2O(a)$ dissociation because the oxygen is easily released to the surface. This orientation was proposed from both experiments and DFT calculations. Kokalj *et al.* [196] have modeled the dissociation of the N_2O molecule by a series of constrained GGA minimization calculations in which the N-O distance was increased stepwise, while all the other structural parameters were optimized.

In Fig. 23, the dissociation profiles are shown for the reaction paths over the on-top and bridge sites at 0.5 and 0.25 ML adsorbate coverages. The height of the dissociation barrier was found to be a function of the adsorbate coverage. In particular, the barrier is reduced upon lowering the adsorbate coverage, the effect being

much more pronounced for the path over the bridge sites than over the on-top sites. The dissociation barrier for the reaction path over the bridge site is lower, despite the fact that the bridge site is less stable. Figure 24 displays the two stable adsorption structures together with the structures of their associated NN-O intermediates immediately after the transition states (TS). The direction of the forces acting on the central N atom and O atom is shown as well. It is worth mentioning that the structural differences between the immediately after TS and the true TS structures are too small to be noticed visually, hence these plots can also serve as structural models for TS.

The DFT-GGA calculations indicate, at least conceptually, that N_2 may desorb in an inclined direction on the non-reconstructed (110) surface. This is due to the bent geometry of the transition-state because the direction of the force acting on the nascent N_2 molecule immediately after the N-O bond rupture is close to the direction of the inclined N-O axis. A tentatively proposed path for N_2O dissociation and N_2 desorption follows the sequence:

$$\textit{on-top } N_2O(a) \rightarrow \textit{bridge } N_2O(a) \rightarrow \text{NN-O}(\textit{TS}) \rightarrow$$
$$\rightarrow N_2(g) + \textit{fcc-hollow } O(a),$$
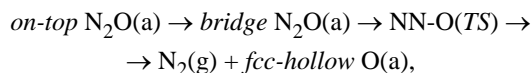
in which the $N_2O(a)$ molecule is first displaced from the on-top to the bridge site and the dissociation then proceeds *via* the elongation of the N-O bond. After the N-O bond is broken, the nascent O(a) is left near the bridge site and eventually stabilizes into an fcc hollow site. A large amount of energy is dissipated during this process, because of the strong oxygen-substrate bonding. The corresponding heat of exothermic reaction *on-top* $N_2O(a) \rightarrow$ *fcc-hollow* $O(a) + N_2(g)$ was estimated to be about -1.0 eV.

8.2.1 Momentum transfer

In the course of the proposed dissociation, after the N-O bond is broken, a repulsive force is acting on the nascent O atom and the N_2 fragment (Fig. 24). To understand the desorption event a step further, the interaction of the nascent N_2 with the substrate should be taken into account. The DFT-GGA calculations predict that the adsorbed N_2 molecule is slightly tilted and prefers the on-top site. The binding energies at 0.5 ML coverage for the c(2×2) surface super-cell are 0.41 and 0.30 eV for the on-top and bridge sites, respectively, while the corresponding N-surface distances are 2.03 and 2.17 Å, respectively. These binding energies and N-surface distances are similar to those of the $N_2O(a)$ admolecule. The N-surface distance slightly smaller for $N_2(a)$ than for $N_2O(a)$ suggests that, during the

N_2O dissociation event, the N_2-surface interaction is attractive and not repulsive, as assumed earlier in the high-energy O atom mechanism based on the *Pauli* repulsion (Section 5.3). The DFT calculations indicate that the basic two parameters determining the N_2 inclined desorption are: (i) the N-O repulsion (here, the bent geometry of the NN-O intermediate is crucial, as it determines the direction of the repulsive forces) and (ii) the N_2-surface attraction. After the N-O bond is broken a repulsive force is acting in an inclined direction on the remaining $N_2(a)$ and $O(a)$ fragments. The force acting on the nitrogen points away from the surface (see Fig. 24); therefore, the N_2 starts to move from the surface. At that moment, an additional force component originating from the surface starts to act on the N_2 and points toward the surface. A consequence of the attractive N_2-surface interaction is therefore an increase in the inclination angle of the N_2 desorption. DFT results thus support the main idea of the mechanism based on the high-energy O atom-assisted desorption, in which the driving force for the inclined N_2 desorption is the momentum received by the N_2 moiety from the high-energy O atom released in the dissociation of $N_2O(a)$ lying on the surface in the [001] direction. A simplified picture of the force components in Fig. 25 shows the difference in the interpretation based on (a) N_2-surface *Pauli* repulsion and (b) DFT-predicted N_2-surface attraction.

9.   SUMMARY

This paper has reviewed the dynamics of nitrogen desorption from catalyst metal surfaces through $N(a)$ recombination, $N(a)$ + $NO(a)$ and $NO(a)$ + $CO(a)$ reactions, NO_2 oxidation/reduction, and N_2O decomposition.

In the recombination reaction (Section 4), desorbing N_2 is mostly hyperthermal and sharply collimates along the surface normal. In addition to the translational form, the vibrational excitation was also observed on Ag, Cu, Ru, and S-promoted Fe. The rotational temperature was commonly close to the surface temperature.

N_2 emission in the NO thermal decomposition on Pd(110) proceeds *via* the $N(a)$ + $NO(a)$ reaction to produce $N_2O(a)$. The decomposition of the $N_2O(a)$ intermediate (Section 5) yields two N_2 desorption channels. A bi-directional distribution of translationally excited N_2 molecules in a plane in the [001] direction is induced by dissociation of $N_2O(a)$ aligned in the [001] direction. In this case, the nascent N_2 molecule desorbs immediately before being accommodated to the surface. In the other channel, N_2 first

accommodates and then desorbs. Its angular distribution follows a simple cosine form. Similar dynamic characteristics were also observed in the N_2O decomposition on Ir(110) and Rh(110) (Sections 5.4 and 5.5) and in the NO + CO reaction under steady-state conditions (Section 6) on Pd(110).

The orientation of N_2O into the [001] direction is supported by DFT calculations and experimental N_2 desorption data. The DFT predicts that N_2O binds weakly to the surface in two alternative forms, either tilted with the terminal N atom attached to the surface or lying horizontally on the surface. The collimation angle and translational energy of desorbing N_2 were proposed to be mainly influenced by the action of the high-energy O atom released in the dissociation of N_2O(a) (Sections 5.3 and 8.2).

Dynamics studies have thrown more light on and opened a new perspective in observing nitrogen removal processes at the atomic and reaction site level. Only for a few systems has the translational, vibrational, and rotational energy of the product molecules been obtained. Partitioning of energy into various degrees of freedom has not been determined yet, and the disposal of energy into the surface coordinates remains unexplained as well. Therefore, further and more systematic analyses of angular and velocity distributions [167] and of state-resolved measurements [31] of desorption of the reaction products are required in nitrogen removal processes on different metals and on different surface structures of the same metal. The interpretation of the experimental results will be necessarily assisted by DFT calculations [195].

ACKNOWLEDGMENTS

References

[1] Lox, E.S.J., and Engler, B.H. 1997, in: Handbook of Heterogeneous Catalysis, G. Ertl, H. Knözinger, and J. Weitkampf (Eds.), VCH Verlagsgesellschaft, Weinheim, Germany, Vol. 4, p. 1633.

[2] Janssen, F. J. 1997, in: Handbook of Heterogeneous Catalysis, G. Ertl, H. Knözinger, and J. Weitkampf (Eds.), VCH Verlagsgesellschaft, Weinheim, Germany, Vol. 4, p. 1559.

[3] Pârvulescu, V., Grange, P., and Delmon, B. 1998, Catal. Today, 46, 233.

[4] Bertelsen, B.I. 2001, Platinum Metals Rev., 45, 50.

[5] Nieuwenhuys, B.E. 2000, Adv. Catal., 44, 259.

[6] Zhdanov, V.P., Kasemo, B. 1997, Surf. Sci. Rep., 29, 31.

[7] Cho, B.K. 1992, J. Catal., 138, 255.

[8] Cho, B.K. 1994, J. Catal., 148, 697.

[9] Belton, D.N., DiMaggio, C.L., Schmieg, S.J., and Ng, K.Y.S. 1995, J. Catal., 157, 559.

[10] Zaera, F., and Gopinath, C.S. 2000, Chem. Phys. Lett., 332, 209.

[11] Ohno, Y., Kimura, K., Bi, M., and Matsushima, T. 1999, J. Chem. Phys., 110, 8221.

[12] Kobal, I., Kimura, K., Ohno, Y., and Matsushima, T. 2000, Surf. Sci., 445, 472.

[13] Matsushima, T. 2002, Catal. Survey from Japan, 5, 71.

[14] Matsushima, T. 1988, Surf. Sci., 197, L287.

[15] Matsushima, T. 1995, Heterogen. Catal. Rev., 2, 51.

[16] Matsushima, T., Yamanaka, T., and Moise, C. 1996, Trends Chem. Phys., 4, 1.

[17] Kobal, I., and Matsushima, T. 1999, Trends Chem. Phys., 7, 169.

[18] Kobal, I., Rzeźnicka, I., and Matsushima, T. 2002, in: Recent Research Developments in Physical Chemistry (Transworld Research Network), in press.

[19] Nørskov, J.K. 1981, J. Vac. Sci. Technol. 18, 420.

[20] Darling, G.R., and Holloway, S. 1994, Surf. Sci., 321, L189.

[21] Darling, G.R., and Holloway, S. 1995, Surf. Sci., 336, L771.

[22] Bradley, T.L., and Stickney, R.E. 1973, Surf. Sci., 38, 313.

[23] Kubiak, D., Sitz, G.O., and Zare, R.N. 1984, J. Chem. Phys., 81, 6397.

[24] Balooch, M., and Stickney, R.E. 1974, Surf. Sci., 44, 310.

[25] Balooch, M., Cardillo, M.J., Miller, D.R., and Stickney, R.E. 1974, Surf. Sci., 46, 358.

[26] van Willingen, W. 1968, Phys. Lett. A, 28, 80.

[27] Doyen, G. 1982, Vacuum, 32, 91.

[28] D'Evelyn, M.P., and Madix, R.J. 1984, Surf. Sci. Rep., 3, 413.

[29] Barker, J.A., and Auerbach, D.J. 1985, Surf. Sci. Rep., 4, 1.

[30] Auerbach, D.J. 1988, in: Atomic and Molecular Beam Methods, G. Scoles (Ed.), Oxford University Press, Oxford, Vol. 1, p. 362.

[31] Hodgson, A. 2000, Prog. Surf. Sci., 63,1.

[32] Rettner, C.T., and Stein, H. 1987, J. Chem. Phys., 87, 770.

[33] Berger, H.F., Leicsh, M., Winkler, A., and Rendulic, K.D. 1991, Chem. Phys. Lett., 175, 425.

[34] Hayden, B.E., and Lamont, C.L.A. 1989, Phys. Rev. Lett., 63,

1823.

[35] Rettner, C.T., Auerbach, D.J., and Michelsen, H.A. 1992, Phys. Rev. Lett., 68, 2547.

[36] Harris, J., Holloway, S., Rahman, T.S., and Yang, K. 1988, J. Chem. Phys., 89, 4427.

[37] Hayden, B.E., and Lamont, C.L.A. 1989, Chem. Phys. Lett., 160, 331.

[38] Hand, M.R., and Holloway, S. 1989, J. Chem. Phys., 91, 7209.

[39] Halstead, D., and Holloway, S. 1990, J. Chem. Phys., 93, 2859.

[40] Gates, G.A., and Holloway, S. 1993, J. Electron. Spectr. Relat. Phenom., 64/65, 633.

[41] Darling, G.R., and Holloway, S. 1995, Rep. Prog. Phys., 58, 1595.

[42] Rettner, C.T., Michelsen, H.A., and Auerbach, D.J. 1995, J. Chem. Phys., 102, 4625.

[43] Dai, J., and Zhang, J.Z.H. 1995, J. Chem. Phys. 102, 6280.

[44] Rettner, C.T., and Auerbach, D.J. 1995, J. Chem. Phys., 104, 2732.

[45] Murphy, M.J., and Hodgson, A. 1998, J. Chem. Phys., 108, 4199.

[46] Groß, A. 1998, Surf. Sci. Rep., 32, 291.

[47] Groß, A., Wilke, S., and Scheffler, M. 1995, Phys. Rev. Let., 1995, 75, 2718.

[48] Dai, J., and Light, J.C. 1997, J. Chem. Phys., 107, 1676.

[49] Kroes, G.J., Baerends, E.J., and Mowrey, R.C. 1997, Phys. Rev. Lett., 18, 3583.

[50] Kroes, G.J. 1999, Prog. Surf. Sci., 60, 1.

[51] Diño, W.A., Kasai, H., and Okiji, A. 2000, Prog. Surf. Sci., 63, 63, and references therein.

[52] Olsen, R.A., Busnego, H.F., Salin, A., Somers, M.F., Kroes, G.J., and Baerends, E.J. 2002, J. Chem. Phys., 116, 3841.

[53] Pijper, E., Kroes, G.J., Olsen, R.A., and Baerends, E.J. 2002, J. Chem. Phys., 117, 5885.

[54] Darling, G.R., and Holloway, S. 1992, J. Chem. Phys., 97, 734.

[55] Michelsen, H.A., Rettner, C.T., and Auerbach, D.J. 1992, Phys. Rev. Lett., 69, 2678.

[56] Hodgson, A., Moryl, J., Traversaro, P., and Zhao, H. 1992, Nature, 356, 501.

[57] Wang, Z.S., Darling, G.R., and Holloway, S. 2002, Surf. Sci., 504, 66.

[58] Anger, G., Winkler, A., and Rendulic, K.D. 1989, Surf. Sci., 220, 1.

[59] Lambert, R.M., Bridge, M.E. 1984, in: The Chemical Physics of Solid Surfaces and Heterogeneous Catalysis, D.A. King, and D.P. Woodruff, (Eds.), Elsevier, Amsterdam, Vol. 3B.

[60] Brown, W.A., King, D.A. 2000, J. Phys. Chem. B, 104, 2578.

[61] Bond, B.C. 1962, Catalysis by Metals, Academic Press, New York.

[62]   Brodén, G., Rhodin, T.N., Benhow, R., and Hurych, Z, 1976, Surf. Sci., 59, 593.

[63]   Hammer, B., Nørskov, J.K. 2000, Adv. Catal. 45, 71.

[64]   Gohndrone, J.M., and Masel, R.I. 1989, Surf. Sci., 209, 44.

[65]   Sugisawa, T., Shiraishi, J., Machihara, D., Irokawa, K., Miki, H., Kodama, C., Kuriyama, T., Kubo, T., and Nozoye, H. 2001, Appl. Surf. Sci., 169-170, 292.

[66]   Sugai, S., Watanabe, T., Kioka, H., and Kawasaki, K. 1991, Surf. Sci., 259, 190.

[67]   Conrad, H., Ertl, G., Küppers, J., and Latta, E.E. 1977, Surf. Sci., 65, 235.

[68]   Sugai, S., Watanabe, T., Miki, H., Kioka, H., and Kawasaki, K. 1990, Vacuum, 41, 90.

[69]   Wickham, D.T., Banse, B.A., and Koel, B.E. 1991, Surf. Sci., 243, 83.

[70]   Ramsier, D.R., Gao, Q., Neergaard Waltenburg, H., and Yates, Jr, J.T. 1994, J. Chem. Phys., 100, 6837.

[71]   Ramsier, D.R., Gao, Q., Neergaard Waltenburg, H., Lee, K.-W., Nooij, O.W., Lefferts, L., and Yates, Jr, J.T. 1994, Surf. Sci., 320, 209.

[72]   Hammer, B. 1998, Faraday Discuss., 110, 323.

[73]   Davies, P.W., and Lambert, R.M. 1981, Surf. Sci., 110, 227.

[74]   Sharpe, R.G., and Bowker, M. 1996, Surf. Sci., 360, 21.

[75]   Pérez Jigato, M., Walter, W.K., and King, D.A. 1994, Surf. Sci., 301, 273.

[76]   Pérez Jigato, M., Somasundram, K., Termath, V., Handy, N.C., and King, D.A. 1997, Surf. Sci., 380, 83.

[77]   Singh, J., Walter, W.K., Atrei, A., and King, D.A. 1991, Chem. Phys. Lett., 185, 426.

[78]   Raval, R., Harrison, M.A., Haq, S., and King, D.A. 1993, Surf. Sci., 294, 10.

[79]   Murray, P.W., Thornton, G., Bowker, M., Dhanak, V.R., Baraldi, A., Rosei, R., and Kiskinova, M. 1993, Chem. Phys. Lett., 71, 4369.

[80]   Fink, T., Dath, J.-P., Basset, M.R., Imbihl, R., and Ertl, G. 1991, Surf. Sci., 245, 96.

[81]   Fink, T., Dath, J.-P., Imbihl, R., and Ertl, G. 1991, J. Chem. Phys., 95, 2109.

[82]   Peden, C.H.F., Goodman, D.W., Blair, D.S., Berlowitz, P.J., Fischer, G.B., and Oh, S.H. 1988, J. Phys. Chem., 92, 1563.

[83]   Zaera, F., and Gopinath G.S. 1999, J. Chem. Phys., 111, 8088.

[84]   Peden, C.H.F., Belton, D.N., and Schmieg, S.J. 1995, J. Catal., 155, 204.

[85]   Vesecky, S.M., Chen, P., Xu, X., and Goodman, D.W. 1995, J. Vac. Sci. Technol. A, 13, 1539.

[86]   Herman, G.S., Peden, C.H.F., Schmieg, S.J., and Belton, D.N. 1999, Catal. Lett., 62, 131.

[87]   Golze, M., Grunze, M., and Unertl, W. 1986, Prog. Surf. Sci., 22, 101, and references therein.

[88]   Kang, D.-B. 1999, Bull. Korean Chem. Soc., 20, 247.

[89]   Zeppenfeld, P., David, R., Ramseyer, C., Hoang, P.N.M., and Girardet, C. 2000, Surf. Sci., 444, 163.

[90]   Bertolo, M., and Jacobi, K. 1992, Surf. Sci., 265, 1.

[91]   Breitschafter, M.J., Umbach, E., and Menzel, D. 1986, Surf. Sci., 178, 725.

[92]   Kuwahara, Y., Jo, M., Tsuda, H., Onchi, M., and Nishijima, M. 1987, Surf. Sci., 180, 421.

[93]   Horn, K., DiNardo, J., Eberhardt, W., Freund, H.-J., and Plummer, E.W. 1982, Surf. Sci., 118, 465.

[94]   Grunze, M., Fuhler, J., Neumann, M., Brundle, C.R., Auerbach, D.J., and Behm, J. 1984, Surf. Sci., 139, 109.

[95]   Raval, R., Harrison, M.A., and King, D.A. 1990, in: The Chemical Physics of Solid Surfaces and Heterogeneous Catalysis, D.A. King and D.P. Woodruff (Eds.), Vol. 3A, Elsevier, Amsterdam, and references therein.

[96]   Rao, C.N.R., and Ranga Rao, G. 1991, Surf. Sci. Rep., 13, 221, and references therein.

[97]   Comelli, G., Dhanak, V.R., Kiskinova, M., Prince, K.C., and Rosei, R. 1998, Surf. Sci. Rep., 32, 165 and references therein.

[98]   Cosser, R.C., Bare, S.R., Francis, S.M., and King, D.A. 1981, Vacuum, 31, 503.

[99]   Auerbach, D.J., Pfnür, H.E., Rettner, C.T., and Schlaegel, J.E. 1984, J. Chem. Phys., 81, 2515.

[100] Pfnür, H.E., Rettner, C.T., Lee, J., Maidx, R.J., and Auerbach, D.J. 1986, J. Chem. Phys., 85, 7452.

[101] Rettner, C.T., and Stein, H. 1990, J. Chem. Phys., 93, 1442.

[102] Thorman, R.P., Anderson, D., and Bernasek, S.L. 1980, Phys. Rev. Lett., 44, 743.

[103] Thorman, R.P., and Bernasek, S.L. 1981, J. Chem. Phys., 74, 6498.

[104] Rettner, C.T., and Stein, H. 1987, Phys. Rev. Lett., 59, 2768.

[105] Kuwahara, Y., Fujisawa, M., Jo, M., Onchi, M., and Nijishima, M. 1987, Surf. Sci., 188, 490.

[106] Murphy, M.J., Skelly, J.F., and Hodgson, A. 1999, J. Chem. Phys., 110, 6954.

[107] Diekhöner, L., Mortensen, H., Baurichter, A., Luntz, A.C., and Hammer, B. 2000, Phys. Rev. Lett., 84, 4906.

[108] Diekhöner, L., Mortensen, H., Baurichter, A., and Luntz, A.C. 2001, J. Chem. Phys., 115, 3356.

[109] Diekhöner, L., Homekær, L., Mortensen, H., Jensen, E., Baurichter, A., Petrunin, V.V., and Luntz, A.C. 2002, J. Chem. Phys., 117, 5018.

[110] Murphy, M.J., Skelly, J.F., and Hodgson, A. 1997, Chem. Phys. Lett., 279, 112.

[111] Murphy, M.J., Skelly, J.F., and Hodgson, A. 1998, J. Chem. Phys., 109, 3619.

[112] Eichler, A., and Hafner, J. 2001, Chem. Phys. Lett., 343, 383.

[113] Nieuwenhuys, B.E., and Sachtler, W.M.H. 1973, Surf. Sci., 34, 317.

[114] Wilf, M., and Dawson, P.T. 1976, Surf. Sci., 60, 561.

[115] Robinson, A.W., Woodruff, D.P., Somers, J.S., Kilcoyne, A.L.D., Ricken, D.E., and Bradshaw, A.M. 1990, Surf. Sci., 237, 99.

[116] Leibsle, F.M., Flipse, C.F.J., and Robinson, A.W. 1993, Phys. Rev. B, 47, 15865.

[117] Moré, S., Berndt, W., Stampfl, C., and Bradshaw, A.M. 1997, Surf. Sci., 381, L589.

[118] Zeppenfeld, P., Diercks, V., Halmer, R., David, R., Pouthier, V., Ramseyer, C., and Girardet, C. 1999, Surf. Sci., 423, 175.

[119] Skelly, J.F., Bertrams, T., Munz, A.W., Murphy, M.J., and Hodgson, A. 1998, Surf. Sci., 415, 48.

[120] Carter, R.N., Murphy, M.J., and Hodgson, A. 1997, Surf. Sci., 387, 102.

[121] Mortensen, J.J., Morikawa, Y., Hammer, B., and Nørskov, J.K. 1997, J. Catal., 169, 85.

[122] Ikai, M., and Tanaka, K. 1999, J. Phys. Chem. B, 103, 8277.

[123] Ikai, M., and Tanaka, K. 1999, J. Chem. Phys., 110, 7031.

[124] Bugyi, L., and Solymosi, F. 1991, Surf. Sci., 258, 55.

[125] Belton, D.N., DiMaggio, C.L., and Ng, K.Y.S. 1993, J. Catal., 144, 273.

[126] Belton, D.N., DiMaggio, C.L., Schmieg, S., and Ng, K.Y.S. 1995, J. Catal., 157, 559.

[127] Ikai, M., He, H., Borroni-Bird, C.E., Hirano, H., and Tanaka, K. 1994, Surf. Sci., 315, L973.

[128] Ikai, M., and Tanaka, K. 1996, Surf. Sci., 357-358, 781.

[129] Comsa, G., David, R., and Schumacher, B.J. 1981, Rev. Sci. Instr., 52, 789.

[130] Colonell, J.I., Gibson, K.D., and Sibener, S. 1996, J. Chem. Phys., 104, 6822.

[131] Ikai, M., Jenssen, N.M.H., Nieuwenhuys, B.E., and Tanaka, K. 1997, J. Chem. Phys., 106, 311.

[132] Jirsak, T., Dvorak, J., and Rodriguez, A. 1999, Surf. Sci., 436, L683.

[133] Peterlinz, K.A., and Sibener, S.J. 1995, J. Phys. Chem., 99, 2817.

[134] Schwalke, U., Parmeter, J.E., and Weinberg, W.H. 1986, J. Chem. Phys., 84, 4036.

[135] Banse, B.A., and Koel, B.E. 1990, Surf. Sci., 232, 275.

[136] Bartram, M.E., Wickham, D.T., and Koel, B.E. 1987, Surf. Sci., 184, 57.

[137] Wickham, D.T., Banse, B.A., and Koel, B.E. 1989, Surf. Sci., 223, 82.

[138] Outka, D.A., Madix, R.J., Fisher, G.B., and DiMaggio, C. 1987, Surf. Sci., 179, 1.

[139] Rodriguez, A. 1990, Surf. Sci., 230, 335.

[140] Guo, X.-C., and Madix, R.J. 2002, Surf. Sci., 496, 39.

[141] Rodriguez, A., Jirsak, T., Dvorak, J., Sambasivan, S., and Fisher, G.B. 2000, J. Phys. Chem. B, 104, 319.

[142] Jirsak, T., Kuhn, M., and Rodriguez, A. 2000, Surf. Sci., 457, 254.

[143] Burch, R., Breen, J.P., and Meunier, F.C. 2002, Appl. Catal. B, in press, and references therein.

[144] Takahashi, N., Shinjoh, H., Iijima, T., Suzuki, T., Yamazaki, K., Yokota, K., Suzuki, H., Miyoshi, N., Matsumoto, S., Tanizawa, T., Tanaka, T., Tateishi, S., and Kasahara, K. 1996, Catal. Today, 27, 63.

[145] Farrauto, R.J., and Heck, R.M. 2000, Catal. Today, 55, 179.

[146] Shelef, M., and McCabe, R.W. 2000, Catal. Today, 62, 35.

[147] Yamazaki, K., Suzuki, T., Takahashi, N., Yokota, K., and Sugiura, M. Appl. Catal. B: Environ., 30, 459.

[148] Olsson, L., Persson, H., Fridell, E., Skoglundh, M., and Andersson, B. 2001, J. Phys. Chem. B, 105, 6895.

[149] Gibson, K.D., Colonell, J.I., and Sibener, S. 1999, Surf. Sci., 443, 125.

[150] Wang, H., Tobin, R.G., DiMaggio, C.R., Fisher, G.B., and Lambert, D.K. 1997, J. Chem. Phys., 107, 9569.

[151] Campbell, C.T., and White, J.M. 1978, Appl. Surf. Sci., 1, 347.

[152] Chin, A.A., and Bell, A.T. 1983, J. Chem. Phys., 87, 3700.

[153] Root, T.W., Schmidt, L.D., and Fisher, G.B. 1983, Surf. Sci., 134, 30.

[154] Root, T.W., Schmidt, L.D., and Fisher, G.B. 1985, Surf. Sci., 150, 173.

[155] Schwartz, S.B., Fischer, G.B., and Schmidt, L.D. 1988, J. Phys. Chem., 92, 389.

[156] Ohno, Y., Kobal, I., Kimura, K., Horino, H., and Matsushima, T. 1999, Catalysts Catal., 41, 421.

[157] Avery, N.R. 1983, Surf. Sci., 131, 501.

[158] Cornish, J.C.L., and Avery, N.R. 1990, Surf. Sci., 235, 209.

[159] Väterlein, P., Krause, T., Bäßler, M., Fink, R., Umbach, E., Taborski, J., Wüstenhagen, V., and Wurth, W. 1996, Phys. Rev. Lett., 76, 4749.

[160] Schwaner, A.L., Mahmood, W., and White, J.M. 1996, Surf. Sci., 351, 228.

[161] Umbach, E., and Menzel, D. 1981, Chem. Phys. Lett., 84, 491.

[162] Spitzer, A., and Lüth, H. 1984, Phys. Rev. B, 30, 3098.

[163] Kodama, C., Orita, H., and Nozoye, H. 1997, Appl. Surf. Sci., 121/122, 579.

[164] Sau, R., and Hudson, J.B. 1981, J. Vac. Sci. Technol., 18, 607.

[165] Hoffman, D.A., and Hudson, J.B. 1987, Surf. Sci., 180, 77.

[166] Li, Y., and Bowker, M. 1996, Surf. Sci., 180, 77.

[167] Horino, H., Rzeźnicka, I., Kokalj, A., Kobal, I., Ohno, Y., Hiratsuka, A., and Matsushima, T. 2002, J. Vac. Sci. Technol., 20, 1592.

[168] Matsushima, T., Shobatake, Y., Ohno, Y., and Tobayashi, K. 1992, J. Chem. Phys., 97, 2783.

[169] Kobayashi, M., and Tuzi, Y. 1979, J. Vac. Sci. Technol., 16, 686.

[170] Ohno, Y., Kobal, I., Horino, H., Rzeźnicka, I., and Matsushima, T. 2001, Appl. Surf. Sci., 169-170, 273.

[171] Horino, H., Liu, S., Hiratsuka, A., Ohno, Y., and Matsushima, T. 2001, Chem. Phys. Lett., 341, 419.

[172] Horino, H., Liu, S., Sano, M., Wako, S., Hiratsuka, A., Ohno, Y., Kobal, I., and Matsushima, T. 2002, Topics Catal., 18, 21.

[173] Haq, A., and Hodgson, A. 2000, Surf. Sci., 436, 1.

[174] Hildenbrand, D.L., and Lau, K.H. 2000, Chem. Phys. Lett., 319, 95.

[175] Sano, M., Ohno, Y., Yamanaka, T., Matsushima, T., Quinay, E.B., and Jacobi, K. 1998, J. Chem. Phys., 108, 10231.

[176] Pedley, J.B., and Marshall, E.M. 1983, J. Phys. Chem. Ref. Data, 12, 967.

[177] Horino, H., and Matsushima, T. 2001, Abstract SS3-Th3, in: Book of Abstracts, 11th International Conference on Solid Surfaces, San Franccisco, USA.

[178] Matsushima, T., Shobatake, Y., Ohno, Y., Nagai, K., and Tobayashi, K. 1991, Chem. Phys. Lett., 187, 277.

[179] Kobal, I., Kimura, K., Ohno, Y., Horino, H., Rzeźnicka, I., and Matsushima, T. 2000, Stud. Surf. Sci. Catal., 130, 1337.

[180] Rzeźnicka, I., Ohno, Y., Horino, H., Kobal, I., Kimura, K., and Matsushima, T. 2000, in: Heterogeneous Catalysis, L. Petrov, C. Bonev, and G. Kadinov (Eds.), (Proc. 9th Int. Symp., Varna 2000), page 97.

[181] Kimura, K., Ohno, Y., and Matsushima, T. 1999, Surf. Sci., 429, L455.

[182] Moula, Md.G., Wako, S., Cao, G., Kimura, K., Ohno, Y., Kobal, I., and Matsushima, T. 1999, Phys. Chem. Chem. Phys., 1, 3677.

[183] Wako, S., Moula, Md.G., Cao, G., Kimura, K., Kobal, I., Ohno, Y., and Matsushima, T. 1999, Langmuir, 16, 2689.

[184] Moula, Md.G., Wako, S., Cao, G., Kobal, I., Ohno, Y., and Matsushima, T. 2001, Appl. Surf. Sci., 169-170, 268.

[185] Maday, T.E., Ramaker, D.E., and Stockbauer, R. 1984, Ann. Rev. Phys. Chem., 35, 215.

[186] Ramsier, R.D., and Yates, Jr., J.T. 1991, Surf. Sci. Rep., 12, 243.

[187] Bourdon, E.B.D., Das, P., Harrison, I., Polanyi, J.C., Segner, J., Stanners, C.D., Williams, R.J., and Young, P.A. 1986, Faraday Discuss. Chem. Soc., 82, 343.

[188] Giorgi, J.B., Künemuth, R., Polanyi, J.C., and Wang, J.-X. 1997, J. Chem. Phys., 106, 3129, see also other papers in this series from I to XV.

[189] Giorgi, J.B., Künemuth, R., and Polanyi, J.C. 1999, J. Chem. Phys., 110, 3129.

[190] Xin, Q.-S., and Zhu X.-Y. 1996, Surf. Sci., 347, 346.

[191] Zhu, X.-Y. 1997, Surf. Sci., 390, 224.

[192] Hammer, B., Hansen, L. B., and Nørskov, J. K. 1999, Phys. Rev. B, 59, 7413.

[193] Perdew, J. P., Burke, K., and Ernzerhof, M. 1996, Phys. Rev.

Let., 77, 3865.

[194] Kokalj, A., Kobal, I., Horino, H., Ohno, Y., and Matsushima, T. 2002, Surf. Sci., 506, 196.

[195] Kokalj, A., Kobal, I., and Matsushima, T. 2002, J. Phys. Chem. B, submitted to publication.

[196] Kokalj, A., Kobal, I., and Matsushima, T. 2002, Extended Abstract TH-P-117 in: Book of Abstracts, 7th International Conference on Nanometer-scale Science and Technology, and 21st European Conference on Surface Science, NANO-7/ECOSS-21, Malmø, Sweden.

[197] Vanderbilt, D. 1990, Phys. Rev. B, 41, 7892.

[198] Horino, H., Wako, S., Matsushima, T., Nagaoka, S., Nakamura, E., Tanaka, S., and Kamada, M. 2000, UVSOR Activity Report, Institute of Molecular Science, Okazaki, Japan, p. 197.

[199] Ceballos, G., Wende, H., Baberschke, K., and Arvanitis, D. 2001, Surf. Sci., 482-485, 15.

[200] Stöhr, J. 1992, NEXAFS Spectroscopy, Springer Series in Surface Science 25, R. Gomer (Ed.), Springer Verlag, Berlin.

[201] Polič, S., Senegačnik, M., Kobal, I., and Zieliński, M. 2001, Polish J. Chem., 75, 1729.

[202] Masson, D.P., Lanzendorf, E.J., and Kummel, A.C. 1995, Phys. Rev. Lett., 74, 1799.

[203] Masson, D.P., Lanzendorf, E.J., and Kummel, A.C. 1995, J. Chem. Phys., 102, 9096.

[204] Redhead, P.A. 1962, Vacuum, 12, 203.

[205] Baroni, S., Dal Corso, A., de Gironcoli, S., and Giannozzi, P. 2001, PWSCF and PHONON: Plane-Wave Pseudo-Potential Codes, http: //www.pwscf.org/.

[206] Kokalj, A. 2000, Doctoral Thesis, Faculty of Chemistry and Chemical Technology, University of Ljubljana, Ljubljana, Slovenia.

[207] Kokalj, A., and Causà, M. 2000, in: Proceedings of High Performance Graphics Systems and Applications, European Workshop, Bologna, Italy, p.p. 51.

[208] Kokalj, A. 1999, J. Mol. Graphics Model., 17, 176.

[209] Kokalj, A., and Causà, M. 2001, XCrySDen: (X-Widows) CRYstalline Structures and DENsities, http: //www-k3.ijs.si/kokalj/xc/.

FIGURE CAPTIONS

Figure 1: Structures of low-index planes of fcc metals and of the stepped surfaces relevant for this review. For the stepped surfaces, side views are also shown [208,209].

Figure 2: *Hartree-Fock* valence eigenvalues and eigenvectors (molecular orbitals) of (a) gas-phase N_2 and (b) gas-phase CO. The labels HOMO and LUMO stand for "highest occupied molecular orbital" and "lowest unoccupied molecular orbital", respectively [208,209].

Figure 3: AR-TDS of N_2, N_2O, and NO in NO decomposition on Pd(110) [11].

Figure 4: (a) Angular distribution of desorbing N_2 in TDS of NO on Pd(110) in the plane along the [001] direction and (b) velocity distributions [11].

Figure 5: Schematic drawings (side views) of the (311), (211), (533), and (755) surfaces of the fcc metals with the microfacet normals. The angles (θ) between the global and microfacet normals are also shown [208,209].

Figure 6: The principle behind the AR-TDS-TOF apparatus. The shape of the chopper is increased.

Figure 7: TDS spectra of N_2 from N_2O-covered Pd(110). The heating rate was 0.6 Ks^{-1}: (a) AI-TDS at various N_2O coverages, Θ_{N_2O}; (b) AR-TDS at $\theta = 52°$ in the plane in the [001] direction for $\Theta_{N_2O} = 0.03$; (c) AR-TDS at $\theta = 55°$ in the plane in the [001] direction for $\Theta_{N_2O} = 0.08$. Deconvolutions shown by dotted curves are based on a *Gaussian* form for each peak. The solid line indicates the sum of all the components [171].

Figure 8: (a) Angular distribution of β_2-N_2 in the plane along the [$1\bar{1}0$] direction of the N_2 emission from N_2O-covered Pd(110). (b) The three-dimensional presentation of spatial distribution of β_2-N_2 [171].

Figure 9: Angular distribution in the plane along the [001] direction of β_1-N_2, β_3-N_2, and β_4-N_2 peaks of N_2 emission from N_2O-covered Pd(110) at Θ_{N_2O}. β_2-N_2 showed a cosine distribution [171].

Figure 10: Velocity distribution of β_1-N_2 at $\theta = -43°$ in the plane in

the [001] direction. Time resolution was 15 μs. The full line is the summation of two modified *Maxwellian* forms shown by broken lines. The dotted line indicates a *Maxwellian* distribution [11].

Figure 11: TDS spectra of N_2 from N_2O-covered Ir(110) at $\Theta_{N2O} =$ 0.15. (a) AI-form, (b) AR-form at $\theta = 0°$, and (c) AR-form at $\theta = 58°$. The heating rate was 3 Ks^{-1}. Deconvolutions shown by dotted curves are based on a *Gaussian* form for each peak. The solid line indicates the sum of all the components [167].

Figure 12: Angular distribution of the β_4-N_2 peak in the plane along the [001] direction of the N_2 emission from N_2O-covered Ir(110) at $T_S = 120$ K and $\Theta_{N_2O} = 0.15$. A typical error level is shown by the inclined bar [167].

Figure 13: TDS spectra of N_2 from N_2O-covered Rh(110) at Θ_{N_2O} = 0.3. (a) AI- form, (b) AR-form at $\theta = 0°$, and (c) AR-form at $\theta = 70°$. The heating rate was 0.6 Ks^{-1}. Deconvolutions shown by dotted curves are based on a *Gaussian* form for each peak. The solid line indicates the sum of all the components [167].

Figure 14: Angular distributions of desorbing N_2 in the plane along the [001] direction on Rh(110). (a) β_1-N_2 at T_S =167 K and Θ_{N_2O} = 0.3. (b) β_4-N_2 at $T_S = 110$ K and $\Theta_{N_2O} = 0.3$. Error bars are also shown [167].

Figure 15: Angular distributions of desorbing N_2 in the [001] direction in NO + CO reaction on Pd(110) under steady-state conditions. (a) At each temperature, data are normalized to the signal at $\theta = 41°$. Full lobular lines represent a $\cos^{28}(\theta + 41°) + \cos^{28}(\theta - 41°)$ distribution. (b) Three-dimensional presentation of the angular distribution of desorbing N_2 [12,13].

Figure 16: Angular distributions of desorbing CO_2 in NO + CO reaction on Pd(110) under steady-state conditions in (a) the [$1\bar{1}0$] direction and (b) the [001] direction. The dotted curves represent typical deconvolutions. (c) Three-dimensional presentation of the fast CO_2 component [12,13].

Figure 17: Velocity distributions of product molecules desorbing in the NO + CO reaction on Pd(110) under steady-state conditions at 540 K. (a) N_2 at $\theta = 41°$; triangles represent raw experimental data and circles represent the signal after subtraction of the *Maxwellian* component at 540 K (dotted line). The full line represents the sum of two components of the modified *Maxwellian* form obtained by

deconvolution (broken lines). (b) N_2O at $\theta = 0°$; experimental points (circles) are well represented by a *Maxwellian* distribution at the surface temperature (solid line). (c) CO_2 at $\theta = 0°$; circles show the experimental data, while broken and dotted lines represent two components obtained by deconvolution of the experimental distribution [12,13].

Figure 18: *Kohn-Sham* valence eigenvalues and eigenvectors (molecular orbitals) of the gas-phase N_2O molecule. The labels HOMO and LUMO stand for "highest occupied molecular orbital" and "lowest unoccupied molecular orbital", respectively. The π orbitals are two-fold degenerated (labeled as (×2)) [208,209].

Figure 19: Top and side views of the *ball-and-stick* models of the GGA-predicted N_2O structures on Pd(110) surface for a (2×2) super-cell representing 0.25 ML coverage. Larger balls are Pd atoms, small blue balls are N atoms, and small red balls are O atoms [208,209,195].

Figure 20: The *ball* model of the GGA-optimized (2×2) horizontal on-top $N_2O(a)$ moiety oriented along the [001] and [$1\bar{1}0$] directions. The left structure is for roughly 0.2 eV/molecule more stable than the right one [208,209,195].

Figure 21: Density of states projected (PDOS) to the N_2O molecule and to the surface Pd atoms that interact with the N_2O molecule. The top panel shows the PDOS for the tilted on-top structure, while the bottom panel shows the PDOS for the horizontal on-top Pd(110)-c(2×2)N_2O structure. The characters of the derived molecular peaks of N_2O are also shown [208].

Figure 22: Charge density difference, $\Delta n(\mathbf{r}) = n_{N_2O/Sub}(\mathbf{r}) - [n_{N_2O}(\mathbf{r}) + n_{Sub}(\mathbf{r})]$, for the tilted on-top structure (left panel) and the horizontal on-top (right panel) Pd(110)-(2×2)N_2O structures. The contours are drawn in a linear scale from -0.02 to +0.02 e/a_0^3, with an increment of 0.005 e/a_0^3. The charge flows from the dark to the bright regions [208,209,195].

Figure 23: The GGA-calculated dissociation profiles of the $N_2O(a)$ molecule. Reaction paths over the on-top and bridge sites are examined at 0.5 and 0.25 ML coverage using the c(2×2) and c(2×4) super-cells, respectively [196].

Figure 24: Optimized structures of the horizontal on-top and bridge $N_2O(a)$ species and the corresponding structures immediately after

the transition state (TS), with the forces (shown as arrows) acting on the central N atom and the O atom [208,209,196].

Figure 25: Force components controlling the inclined desorption of N_2 in the dissociation of $N_2O(a)$ lying in the [001] direction on the Pd(110) surface (a) based on N_2-Pd *Pauli* repulsion and (b) based on the DFT-predicted N_2-Pd attraction [196,13].

Table 1: The DFT-GGA-calculated binding energies (E_b) and structural parameters of $N_2O(a)$ adsorbed on Pd(110) for several surface super-cell geometries representing 0.5 ML and 0.25 ML coverage. The labels d_{PdN}, d_{NN}, d_{NO}, and d_{PdO} stand for the distances between the corresponding atoms. The labels $\angle_{Pd*NN}$, $\angle_{NNO}$, and $\angle_{NO*Pd}$ stand for the corresponding angles. The symbol Pd* (or *Pd) stands for either the Pd atom (i.e., for on-top structures) or the midpoint between the two bridging Pd atoms (i.e., for bridge structures). Hence, the symbol $\angle_{Pd*NN}$ corresponds to the Pd-N-N angle for the on-top structures, while, for the bridge structures, it corresponds to the angle between the "bridge-midpoint"-N-N [194,195].

Super-cell	Site	E_b (eV)	d_{PdN} (Å)	d_{NN} (Å)	d_{NO} (Å)	d_{PdO} (Å)	$\angle_{Pd*NN}$ (°)	$\angle_{NNO}$ (°)	$\angle_{NO*Pd}$ (°)
c(2×2)	tilted on-top	0.39	2.11	1.15	1.21		150	179	
	horizontal on-top	0.38	2.10	1.17	1.24	2.33	130	156	116
	tilted bridge	0.32	2.23	1.16	1.21		160	178	
	horizontal bridge	0.18	2.28	1.18	1.25	2.62	136	153	120
(2×2)	tilted on-top	0.36	2.09	1.15	1.21		157	180	
	horizontal on-top	0.40	2.07	1.17	1.23	2.27	132	151	121
	tilted bridge	0.29	2.22	1.16	1.21		160	178	
	horizontal bridge	0.27	2.13	1.20	1.32	2.30	143	135	132
$N_2O(g)$				1.14	1.21			180	

Fcc Low Index Surfaces
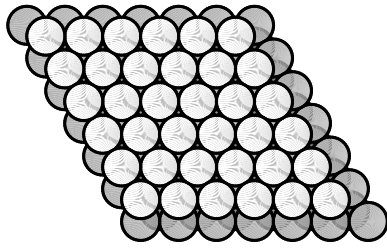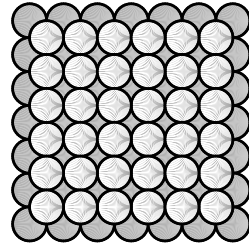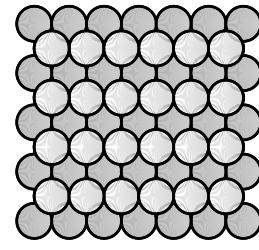
(111) (100) (110)

Fcc Stepped Surfaces
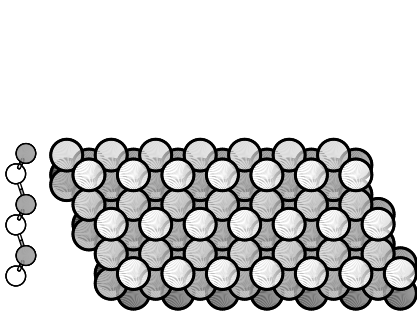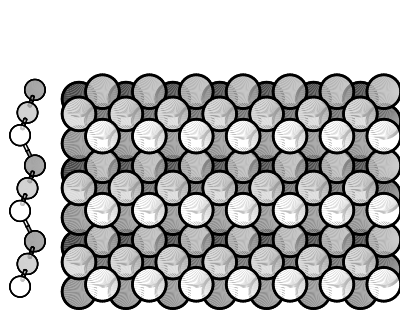
(210) = [(S)2(100) × (110)] (310) = [(S)3(100) × (110)] (410) = [(S)4(100) × (110)]
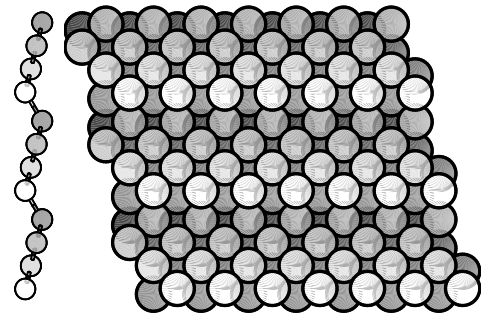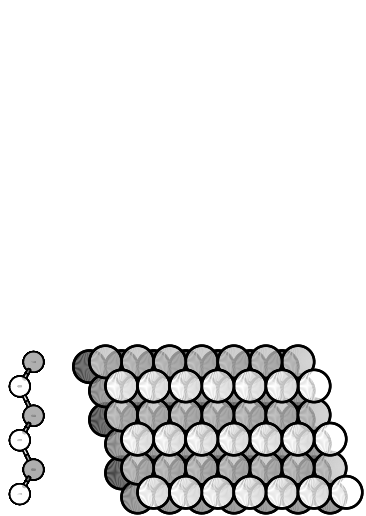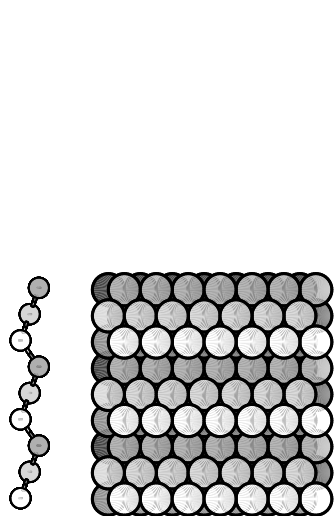
(311) = [(S)2(111) × (100)] (211) = [(S)3(111) × (100)] (533) = [(S)4(111) × (100)] (755) = [(S)6(111) × (100)]
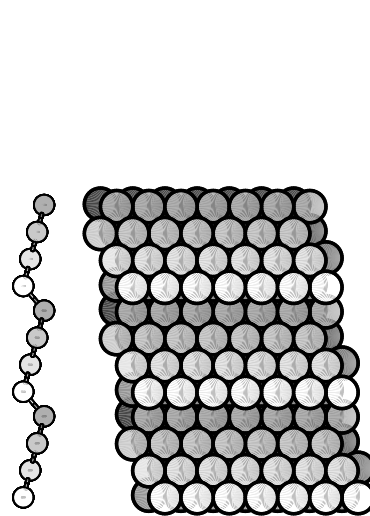
Fig. 1 I. Kobal *et al.*, Trends Chem. Phys.

$3\sigma_g$&$1\pi_u$

$2\sigma_g$

$2\sigma_u$

$1\pi_g$

E / eV

$2\sigma_g$ $2\sigma_u$ $3\sigma_g$ $1\pi_u$ (2×) (HOMO) $1\pi_g$ (2×) (LUMO)

(a) Eigenvalues and Eigenvectors of $N_2(g)$

1π

2π

3σ

4σ

5σ

E / eV

3σ 4σ 1π (2×) 5σ (HOMO) 2π (2×) (LUMO)
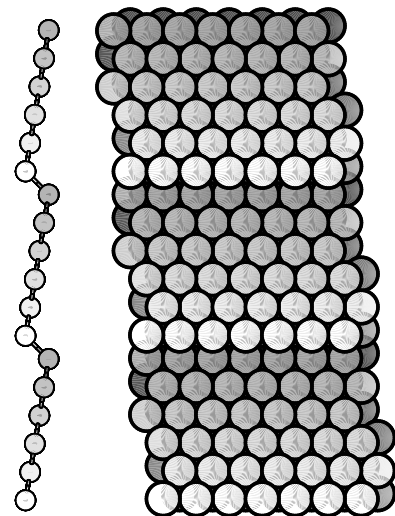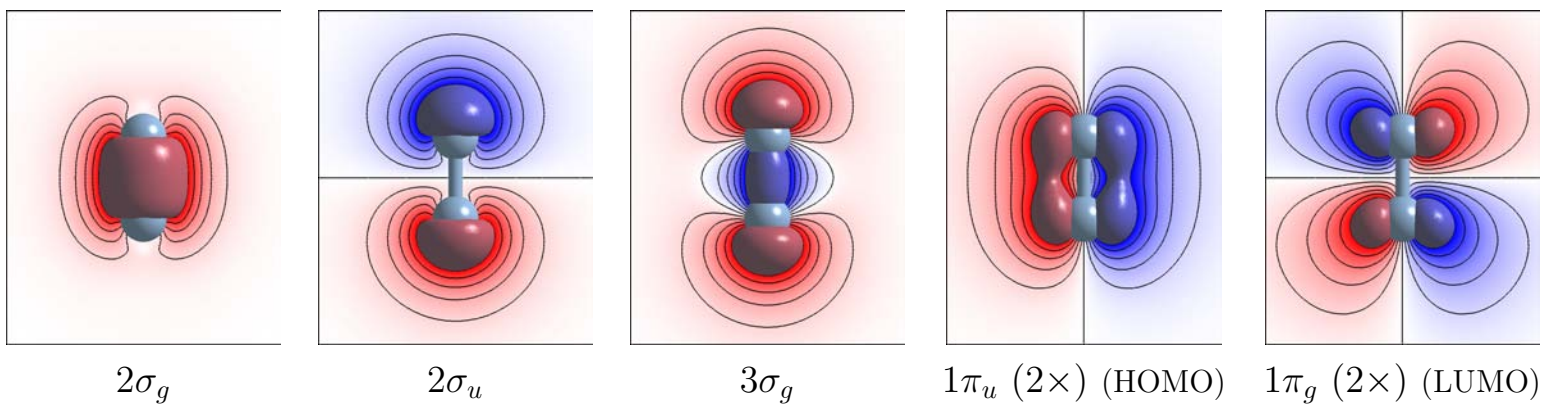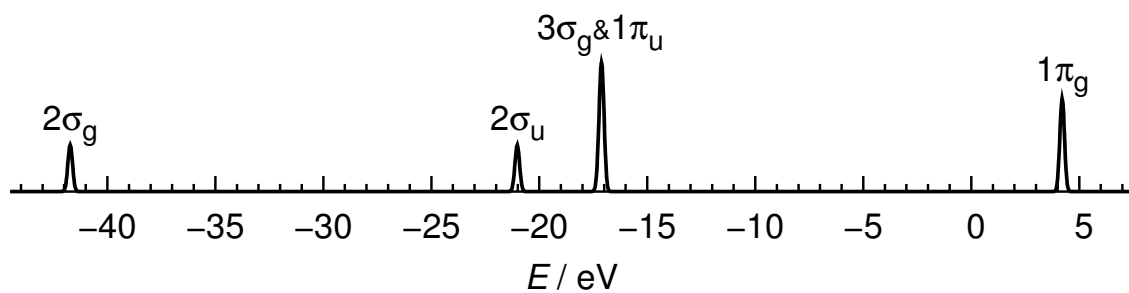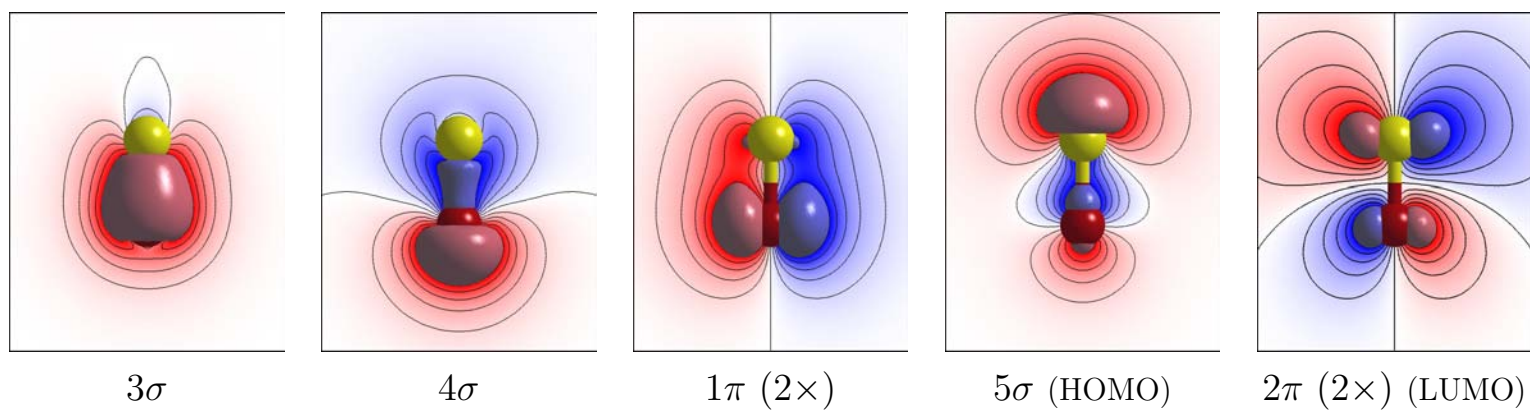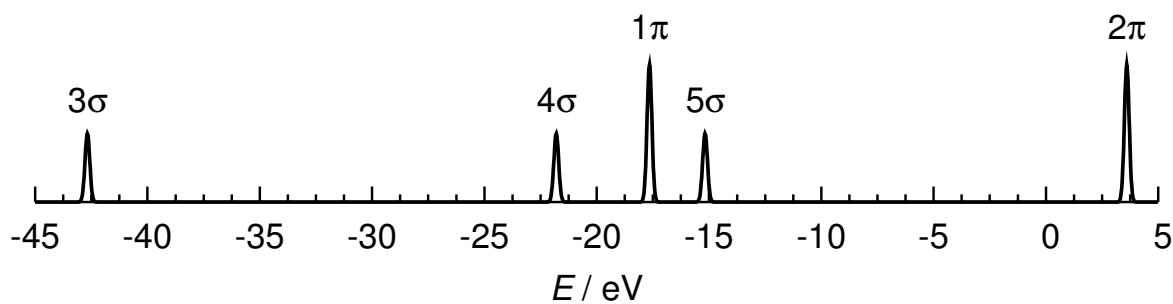
(b) Eigenvalues and Eigenvectors of $CO(g)$

Fig. 2   I. Kobal *et al.*, Trends Chem. Phys.

AR Mass Signal (arb. units)

0.50L NO

N_2

41°

0°

N_2O

NO

Fig. 3

Temperature / 100K

NO / Pd(110)

Fig. 4

$\theta = 0^o$
[311]
$\theta = -25.3^o$ $\theta = 29.5^o$
[100]   [111]

(311)

$\theta = 0^o$
[211]
$\theta = -35.3^o$ $\theta = 19.5^o$
[100]   [111]

(211)

$\theta = 0^o$
[533]
$\theta = -40.3^o$ $\theta = 14.4^o$
[100]   [111]

(533)

$\theta = 0^o$
[755]
$\theta = -45.3^o$ $\theta = 9.4^o$
[100]   [111]

(755)

Fig. 5

Analyzer **Chopper House** **Reaction Chamber**

flight path →
30.4cm

LEED-AES

Ionizer

Slit

Pulse Counting

Mass

Sample

Mass

Chopper

Ion Gun

Trigger

⇓ ⇓ ⇓

| ion Pump +cryo-pump | ion Pump +cryo-pump | ion Pump |

← **cross-correlation chopper**

Fig. 6

Fig. 7

(a)

θ / Intensity

N$_2$O / Pd(110)

0

β_2-N$_2$

cos θ

−90

90

[$\bar{1}$10]

[1$\bar{1}$0]

(b)

$_2$-N$_2$

$_1$-N$_2$

[1$\bar{1}$0]

[001]

Fig. 8

θ in [001]

(a) $\Theta_{N_2O} = 0.03$

β_4
$\cos^{28}(\theta \pm 50)$

0.04

0.02

(b) $\Theta_{N_2O} = 0.2$

β_3
$\cos^{50}(\theta \pm 43)$

0.5

0.3

0.2

β_4
$\cos^{50}(\theta \pm 44)$

(c) $\Theta_{N_2O} = 1.0$

β_3
$\cos^{30}(\theta \pm 43)$

1.0

0.5

β_1
$\cos^{50}(\theta \pm 43)$

[00$\bar{1}$] [001]

Fig. 9

N₂O / Pd(110)

β₁–N₂

$T_{<E>}$

1930K

152K

580K

$\theta = -43°$

Mass Signal (arb. u.)

Velocity / km s⁻¹

Fig. 10

(a) AI

Ir(110)

$\Theta_{N_2} \approx 0.15$

β_4 β_3 β_2 β_1

(b) AR : 0°

$^{15}N_2$ Signal / arb. units

(c) AR : 58°

β_4 β_3 β_2 β_1

T_s / K

Fig. 11

θ in [001] direction

Ir(110) β_4-N_2 $\Theta_{N_2} \approx 0.15$

$\cos\theta$

$\cos^{15}(\theta\pm65)$

Fig. 12

(a) AI Rh(110)

$\Theta_{N_2} \approx 0.3$

β_4 β_3 β_2 β_1

(b) AR : 0°

$^{15}N_2$ Signal / arb. units

(c) AR : 70°

β_4 β_3 β_2 β_1

T_s / K

Fig. 13

θ in [001] direction

(a) Rh(110)

$_1$-**N$_2$**

cos

(b)

$_4$-**N$_2$**

$_{N_2}$ ≈ 0.3

$\cos^{15}(\pm 70)$

[00$\bar{1}$]   [001]

Fig. 14

(a) $\theta = 0$ NO+CO / Pd(110)

−41

41

N₂

−90

90

[00$\bar{1}$]

[001]

Ts/K=500( ), 510( ), 520( ), 540( ), 550( ),

570( ), 600( ) and 620( )

(b)

N₂

N₂

[1$\bar{1}$0]

[001]

Fig. 15

(a) $\theta = 0°$ NO+CO / Pd(110)

$\cos^3 \theta$

$\cos \theta$

CO$_2$

$T_S = 540$K

-90° [$\bar{1}$10]   [1$\bar{1}$0] 90°

(b) $\theta = 0°$

$\cos^{15} \theta$

$\cos \theta$

CO$_2$

$T_S = 540$K

-90° [00$\bar{1}$]   [001] 90°

CO$_2$

[1$\bar{1}$0]

[001]

Fig. 16

Fig. 17

4σ 5σ 6σ 1π(2×) 7σ 2π(2×)
(HOMO) 3π(2×)
(LUMO)
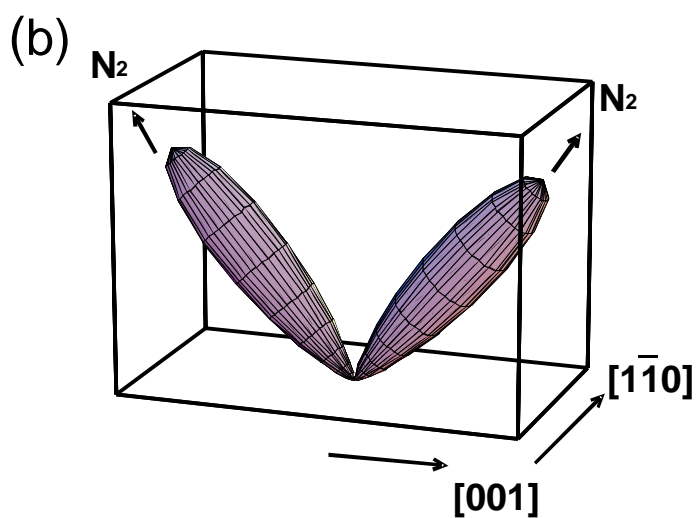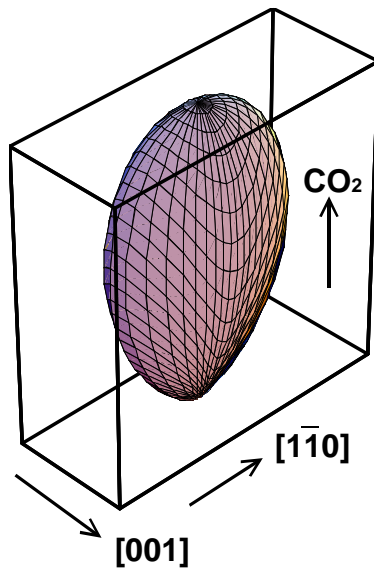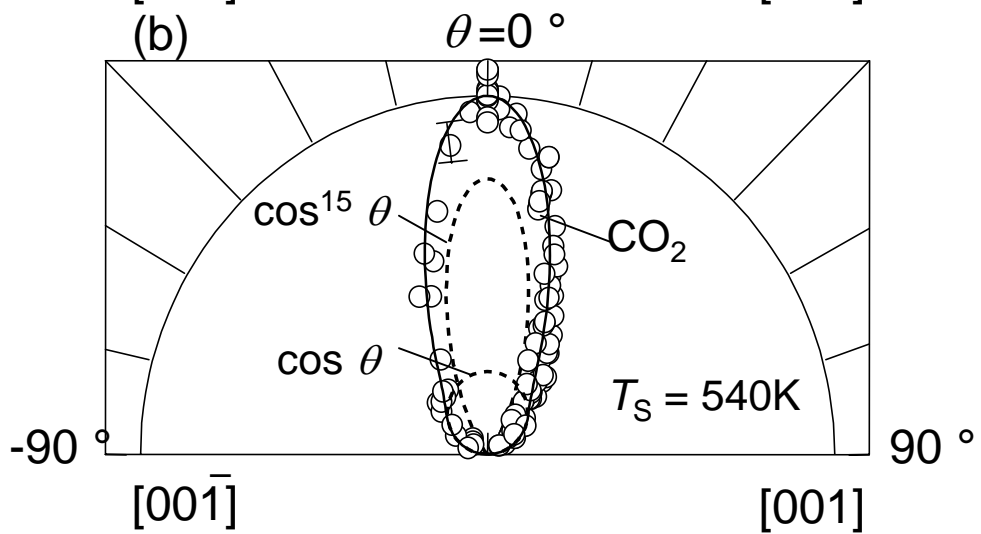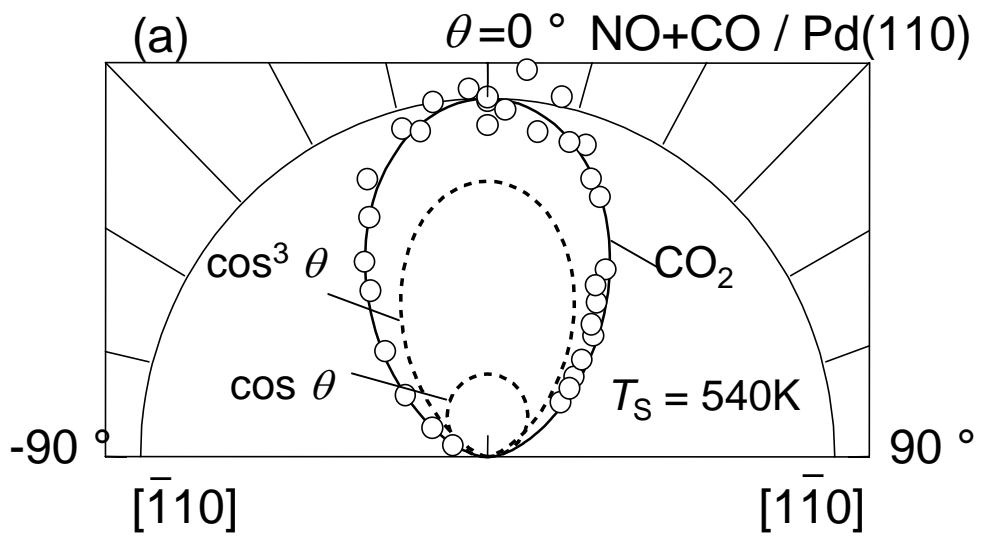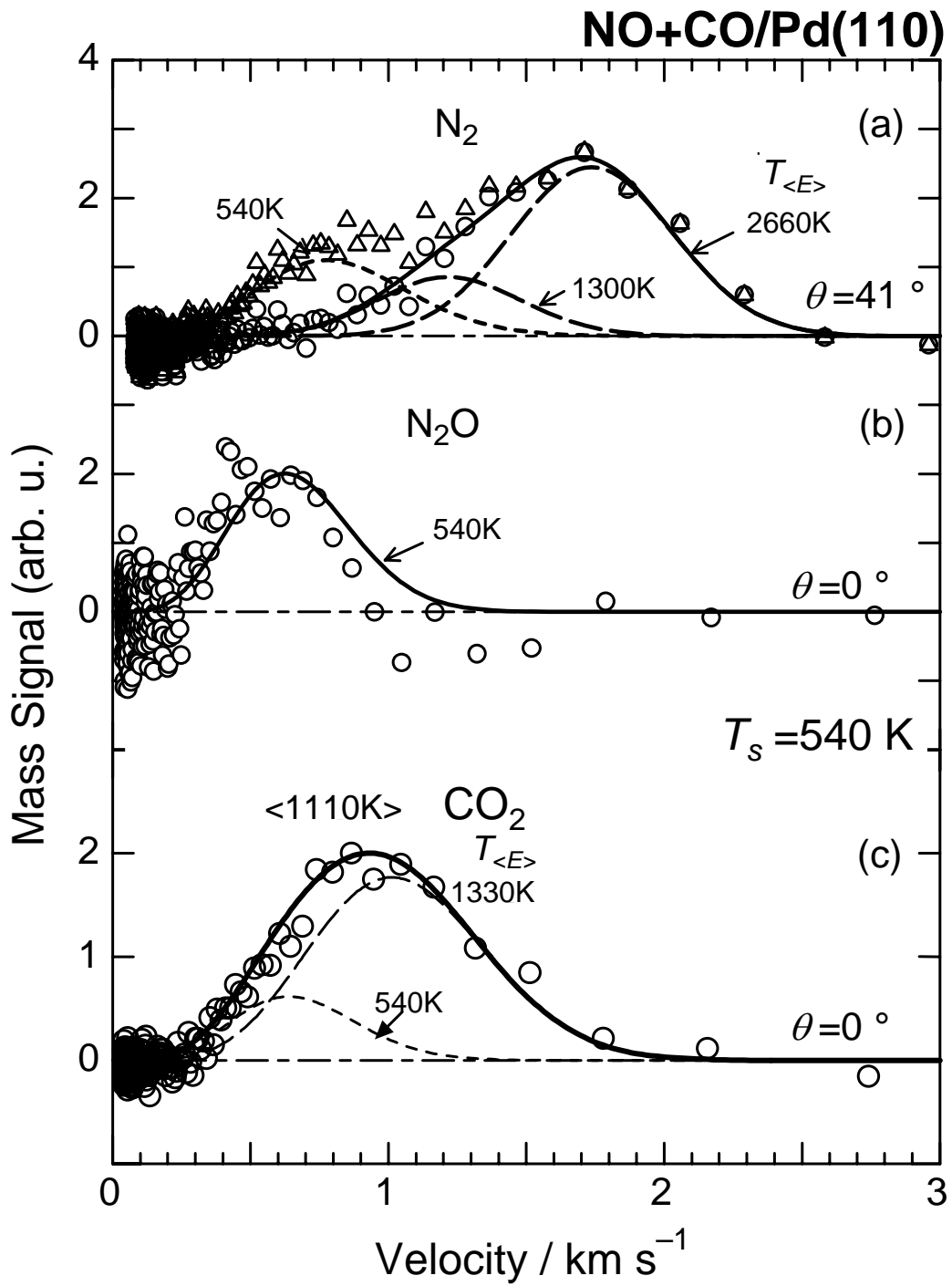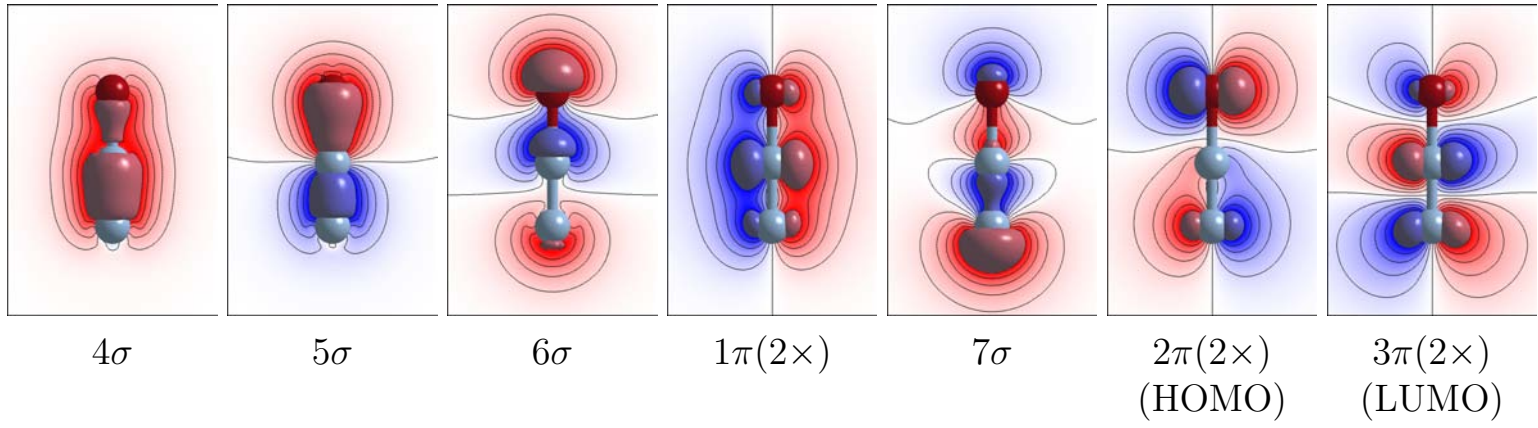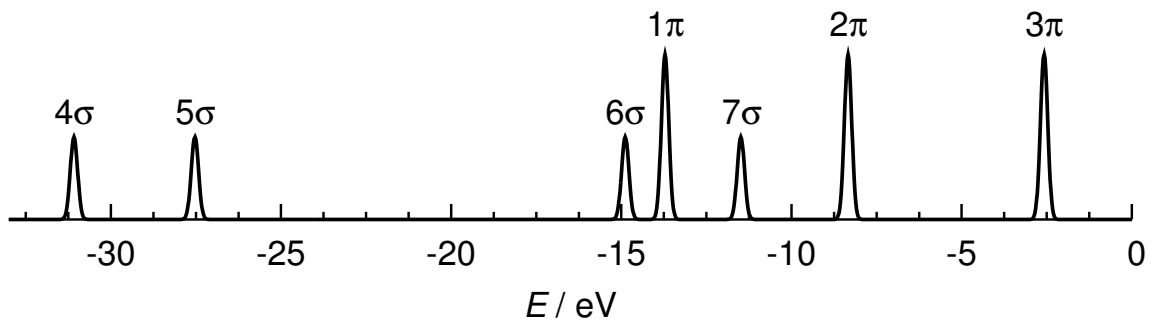
Fig. 18   I. Kobal *et al.*, Trends Chem. Phys.

Pd(110)–(2 × 2)N$_2$O			
tilted on-top	*horizontal on-top*	*tilted bridge*	*horizontal bridge*
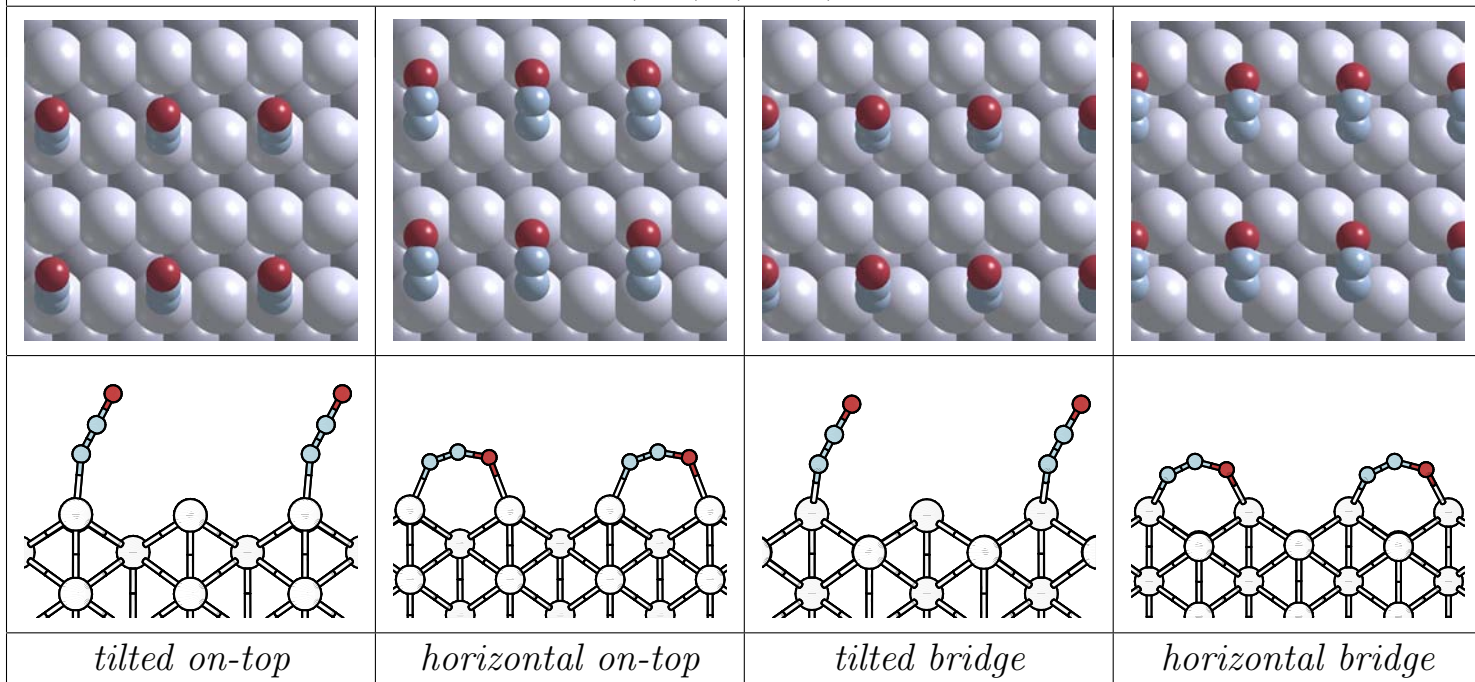
Fig. 19   I. Kobal *et al.*, Trends Chem. Phys.
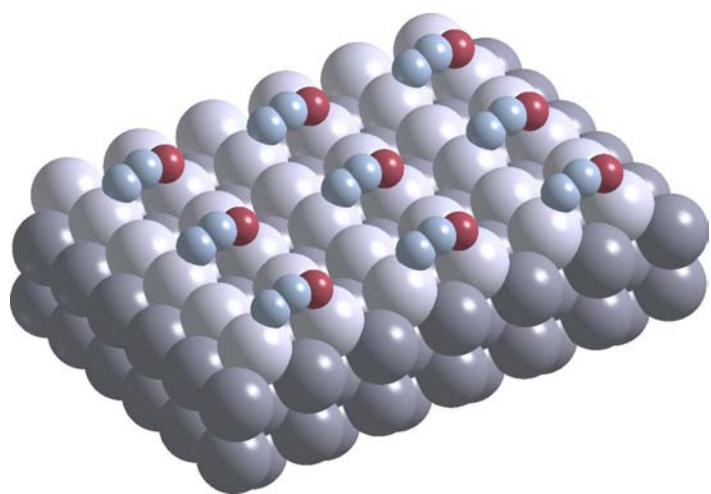
along [001]
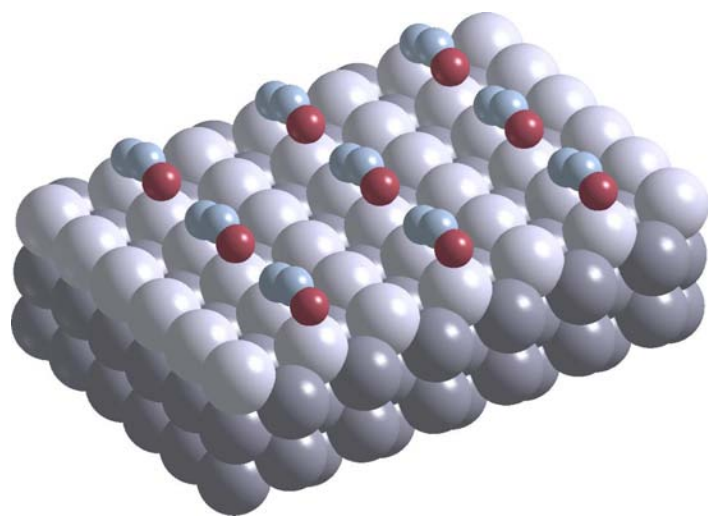
along [1$\bar{1}$0]

Fig. 20

I. Kobal *et al.*, Trends Chem. Phys.
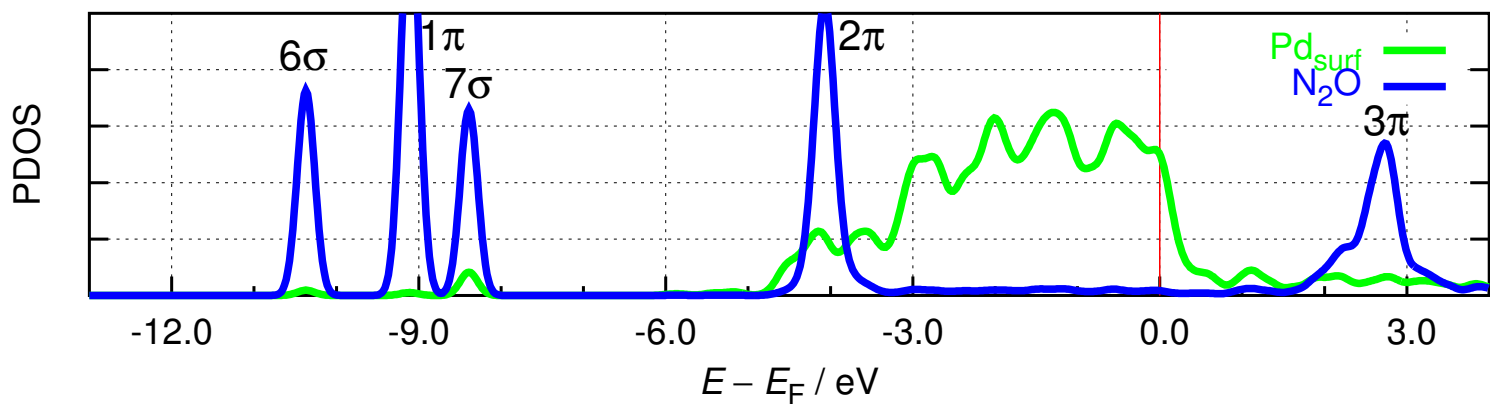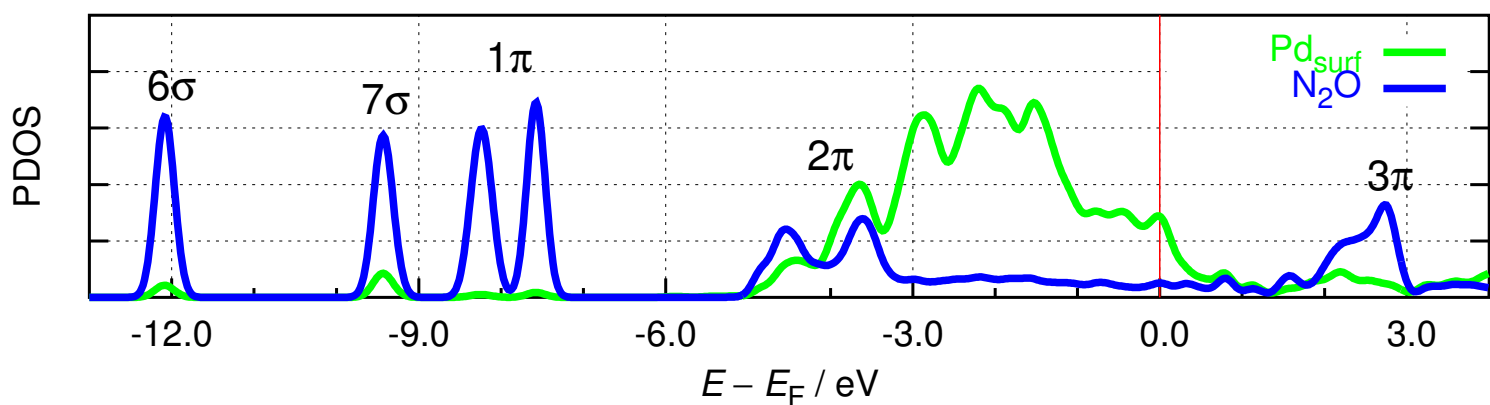
tilted on-top $N_2O(a)$

horizontal on-top $N_2O(a)$

Fig. 21   I. Kobal *et al.*, Trends Chem. Phys.

tilted on-top $N_2O(a)$ *horizontal on-top* $N_2O(a)$
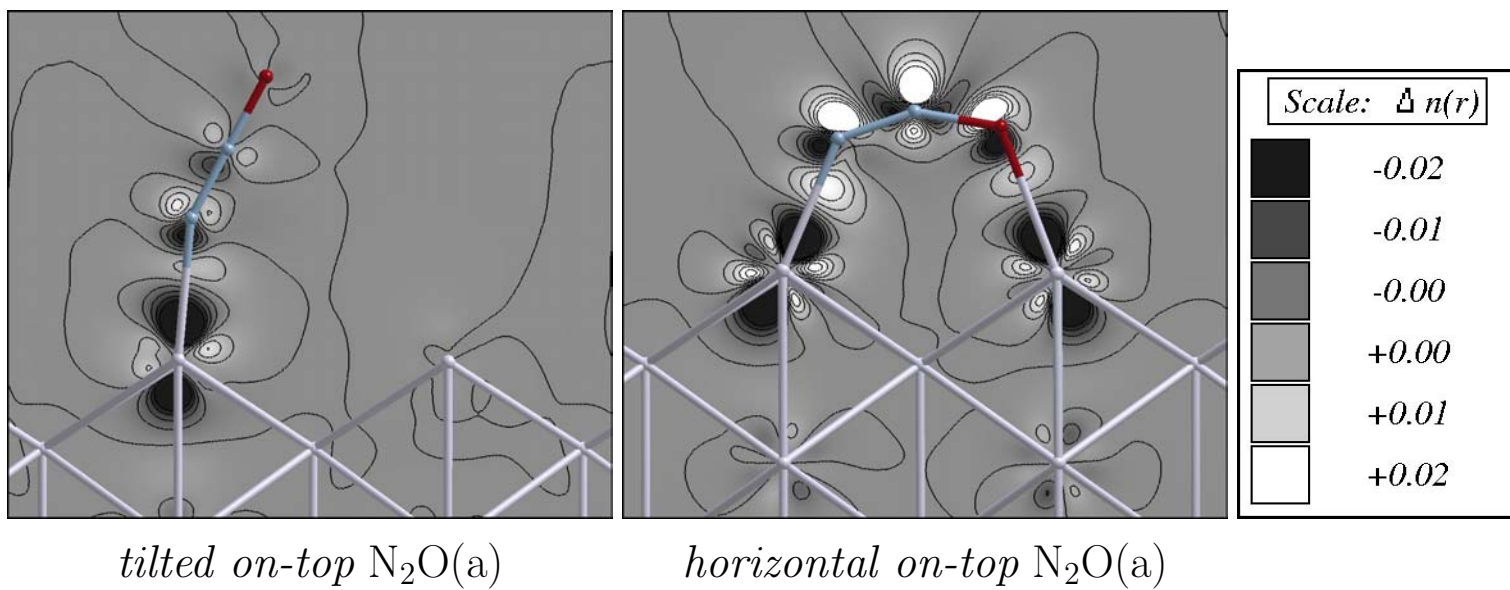
Fig. 22

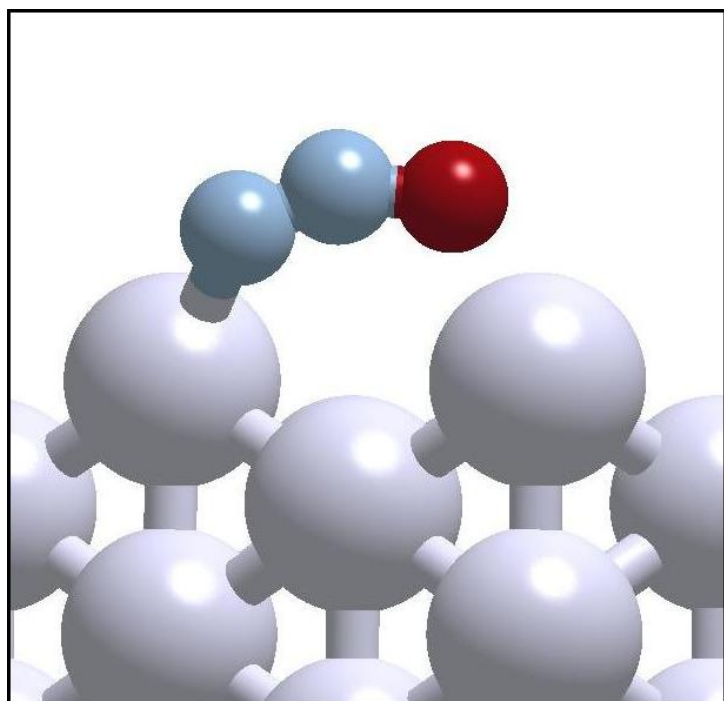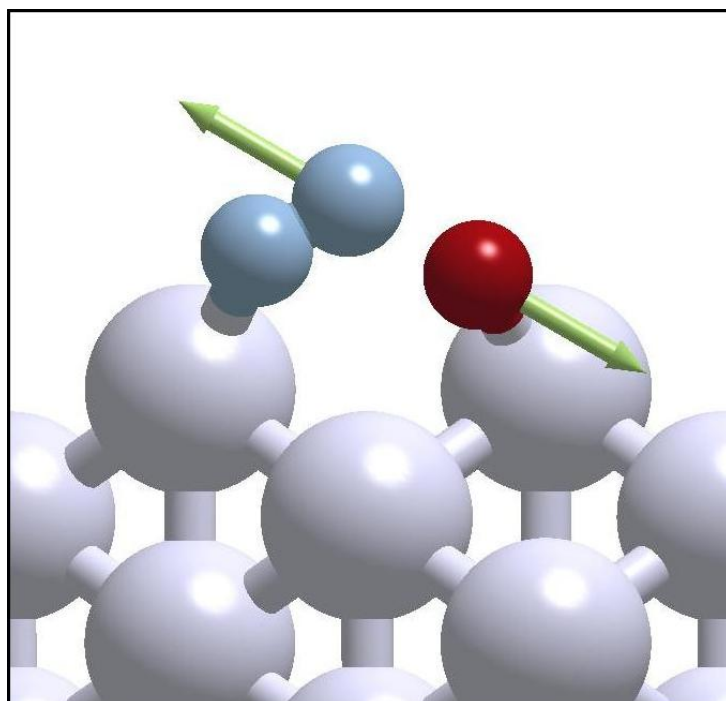**Fig. 23**   I. Kobal *et al.*, Trends Chem. Phys.
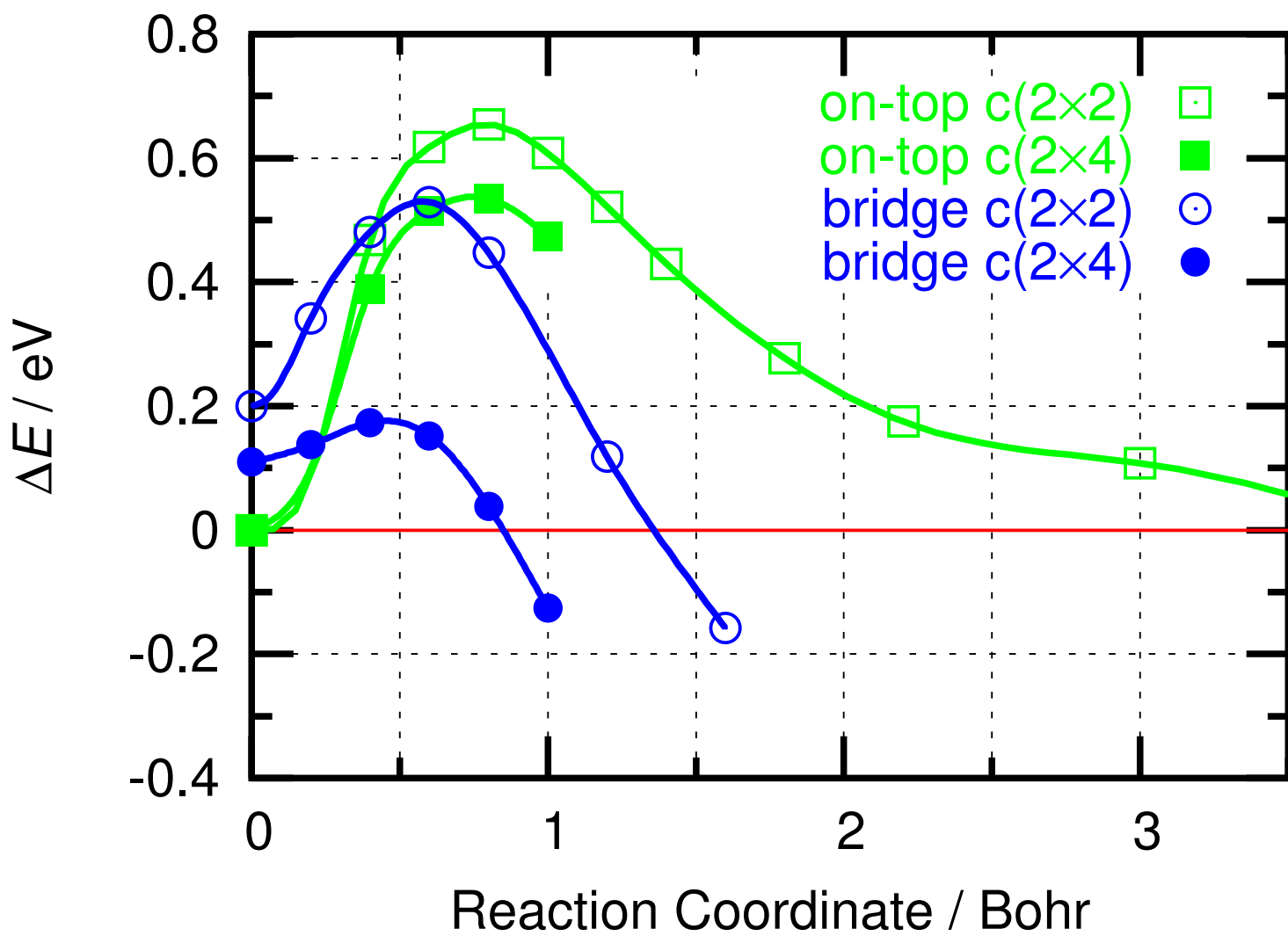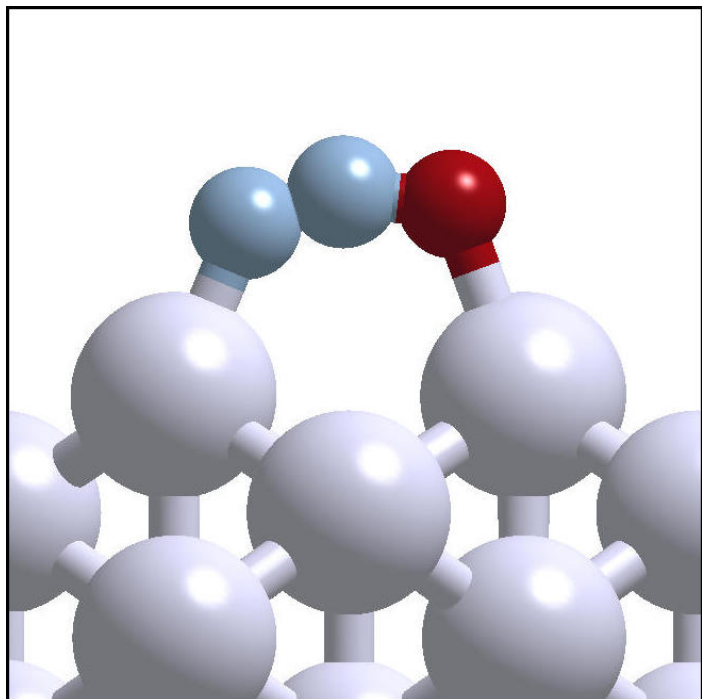
horizontal on-top $N_2O(a)$
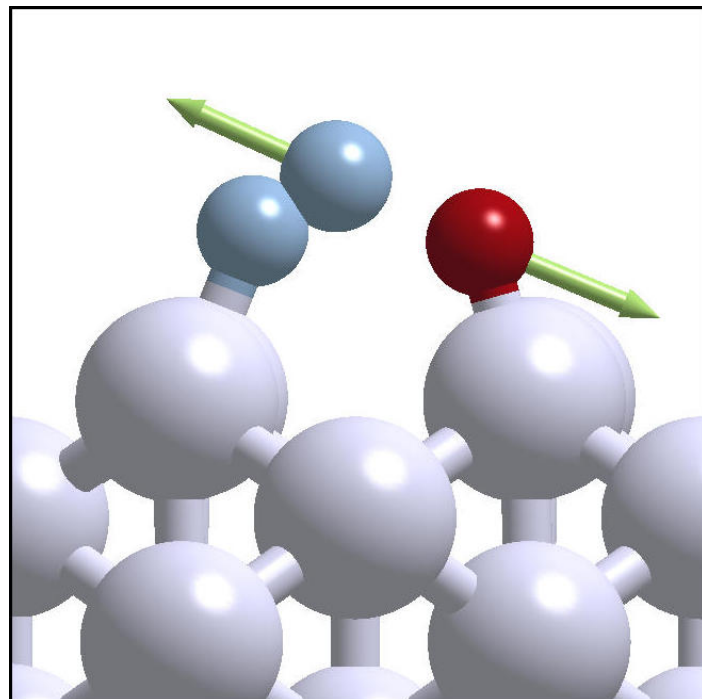
on-top after–TS

horizontal bridge $N_2O(a)$

bridge after–TS
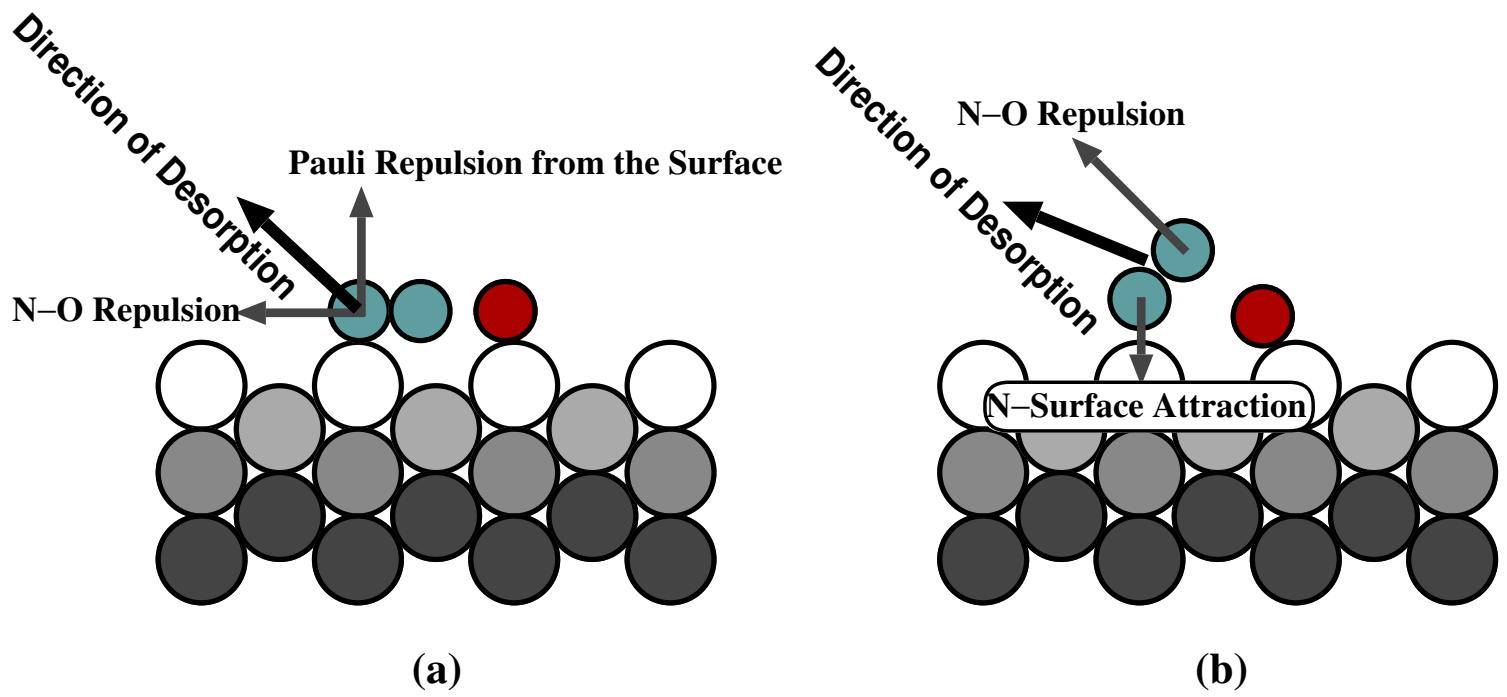
Fig. 24

I. Kobal *et al.*, Trends Chem. Phys.

(a)

(b)

Direction of Desorption

Pauli Repulsion from the Surface

N−O Repulsion

N−O Repulsion

N−Surface Attraction

Fig. 25